Mercury speciation in a tropical soil association; Consequence of gold mining on Hg distribution in French Guiana

Stéphane Guédron, Sylvain Grangeon, Bruno Lanson, Michel Grimaldi

Mercury speciation in a tropical soil association;

Consequence of gold mining on Hg distribution in French Guiana.

Stéphane GUEDRON[a,*], Sylvain GRANGEON[b], Bruno LANSON[b], and Michel GRIMALDI[c].

[a] Environmental Geochemistry Group - LGIT, Observatory of Earth and Planetary Science (OSUG), University of Grenoble / CNRS - Maison des Géosciences, 1381, rue de la Piscine - Domaine Universitaire - 38400 Saint-Martin-D'Hères, France.

[b] Mineralogy & Environments - LGCA, Observatory of Earth and Planetary Science (OSUG), University of Grenoble / CNRS - Maison des Géosciences, 1381, rue de la Piscine - Domaine Universitaire - 38400 Saint-Martin-D'Hères, France.

[c] UMR Bioemco- Biogéochimie et Ecologie des Milieux Continentaux, UMR211, Institut de Recherche pour le Développement, 32 avenue Henri Varagnat, 93143 Bondy, France.

[*] Corresponding author – Present address: Institut F.A.-Forel, route de Suisse 10, CP416, 1290 Versoix, Switzerland.

E-mail: stephane.guedron@unige.ch

Tel : +41-223-790-311

Fax : +41-223-790-329

Abstract.

Mercury (Hg) speciation was compared in French Guiana pristine soils and in Hg contaminated soils impacted by former (~1950's) gold-mining activities which used Hg for gold amalgamation. Four selective extractions were performed on soil samples to assess the fraction of Hg present as Hg(II) and bond to organic matter (extracted by NH_4OH and KOH), to amorphous iron oxides (ascorbate) and to soil components other than refractory minerals (HCl/HNO_3). In addition, pyrolysis was used to quantify the content of elemental Hg in contaminated soils. X-ray diffraction (XRD) and X-ray fluorescence micro-mapping (μXRF) were used in combination to selective extractions to assess the nature of targeted components, the possible overlaps between the different extraction procedures and the spatial correlation between Si, K, Fe, Au and Hg.

In soil profiles from pristine toposequences, Hg concentrations (0.01-0.49 $\mu g.g^{-1}$) decreased with increasing depth in soil matrix. Hg concentrations also decreased from ferralsols to acrisols and further to gleysols. In pristine soil matrix, Hg was mainly associated to the clay size fraction (< 2 μm) which was mainly constituted of amorphous and crystalline Fe oxides (Al-substituted goethite and hematite), gibbsite and fine organic matter (OM), whose relative abundances vary along the soil association. Total Hg concentration was positively correlated with sulfurs and organic carbon suggesting the association of Hg with OM sulfur-bearing functional groups. Gleysols were depleted in Hg because of the prevailing reducing conditions that lead to the dissolution of iron oxides. In the same soil profiles, Hg concentrations in ferruginous nodules, which make up most of the soil coarse fraction (> 2 mm), were similar to those reported in the pristine soil matrix. These nodules mainly contained Al-substituted hematite and goethite and were especially abundant upslope in

48 ferralsols and acrisols. Gold-mined gleysols were strongly disorganized by former
49 activities as neither the original structure nor the texture was preserved. Soil
50 granulometry was dominated by gravels, sands and silts. Hg concentrations (0.09-
51 9.22 $\mu g.g^{-1}$) largely exceeded those in pristine soils. μXRF allowed the identification
52 of Au-amalgamated Hg and of elemental Hg droplets. Pyrolysis confirmed Hg to be
53 mainly present in its elemental form in contaminated soils. Selective extractions
54 showed additional minor contributions of Hg(II) associated to OM, and to Al or Fe
55 oxides.

56 The combination of selective extractions with XRD and μXRF data showed
57 that extraction efficiency is strongly dependent on the soil type, and that this
58 efficiency needs to be determined on a soil-by-soil basis for Hg speciation studies.
59 KOH extraction was especially delicate as crystalline and amorphous oxides were
60 extracted together with organic matter.

61 Key-words: Mercury, Tropical soils, French Guiana, gold-mining, XRD, selective
62 extraction, speciation.

63 **1. Introduction**

64 Tropical soils from the Amazonian basin are known to have accumulated
65 atmospheric Hg over millions of years, thus inducing geochemical backgrounds
66 higher than those reported in boreal and temperate climate soils (Carmouze et al.,
67 2001). In addition, past and current gold mining activities, which represent the main
68 contribution to anthropogenic emissions (Lacerda, 1997; Roulet et al., 1998; Guedron
69 et al., 2006), contribute to increase further the total Hg concentrations in these soils.
70 Small-scale mining activities have increased significantly during the worldwide gold
71 rush, created by the gold price increase in the 1980's. UNIDO (United Nations
72 Industrial Development Organization) estimates that in 2004 10 to 15 million people
73 were working in small-scale gold mines releasing 650-1000 tons of Hg annually
74 (Veiga and Baker, 2004). In addition to this major atmospheric emission, gold mining
75 activities release large amounts of Hg-rich particles into hydrosystems where
76 methylmercury (MMHg) production has been clearly identified in anoxic and suboxic
77 areas (Benoit et al., 2003; Coquery et al., 2003). In turn, MMHg accumulation along
78 the aquatic food chains is a threat to Amerindian populations whose diet relies mainly
79 on fish (Lebel et al., 1996; Frery et al., 2001; Barbosa et al., 2003). To assess Hg
80 mobility and its availability to methylating microorganisms, it is thus crucial to
81 determine how Hg is bond to soil particles.

82 The retention capacity of tropical soils varies as a function of soil components
83 which depends on soil types and horizons (Charlet and Sposito, 1987; Charlet and
84 Sposito, 1989; Fontes and Gomes, 2003). In particular, the relative proportions of soil
85 components responsible for Hg retention [clay minerals, Fe-, Al-, and Mn-
86 (oxyhydr)oxides, organic matter] vary with the geochemical conditions which in turn

87 depend on the topographic position along the soil association (Boulet et al., 1993; do
88 Valle et al., 2005; Fritsch et al., 2005; Fritsch et al., 2006).

89 Hg has a high affinity for soil organic matter, especially for reduced sulfur
90 groups such as thiol ligands (Schuster, 1991; Skyllberg et al., 2000; Khwaja et al.,
91 2006; Skyllberg et al., 2006). High Hg levels can also be associated to Fe-
92 (oxyhydr)oxides. In particular, amorphous or poorly crystalline oxides are known as
93 sinks for metal contaminants owing to their large surface area and/or microporous
94 structure (Trivedi and Axe, 2001). Ferruginous nodules, formed during the lateritic
95 weathering process, also contain elevated Hg contents (Roulet and Lucotte, 1995;
96 Roulet et al., 1998; De Oliveira et al., 2001; Brabo et al., 2003).

97 Solid-phase chemical speciation has been widely used on sediment samples
98 to decipher metal distribution in contaminated systems (Wallschlager et al., 1998;
99 Rodriguez Martin-Doimeadios et al., 2000; Beldowski and Pempkowiak, 2003; Bloom
100 et al., 2003; Boszke et al., 2006). Most of the recent studies of Hg speciation in
101 natural or contaminated sediments, soils and tailings used sequential extraction
102 procedure (SEP) or Hg pyrolysis procedure following published recommendations
103 (Eagenhouse et al., 1978; Di Giulio and Ryan, 1987; Biester and Scholz, 1997;
104 Bloom et al., 2003). While some studies strictly follow the described SEP (Sanchez et
105 al., 2005; Beldowski and Pempkowiak, 2007), many authors adapt it to the studied
106 matrix. Each extraction step of the SEPs for soils and sediments is critical, as it is
107 challenging to obtain an adequate recovery by preventing losses, contamination or
108 speciation changes, and limiting the interferences (Leermakers et al., 2005).

109 In the present study, the speciation of Hg among soil components was
110 determined in soil profiles along pristine soil toposequences and in soils
111 contaminated with Hg by former gold mining in a French Guiana watershed.

112 Separate selective extractions were used to quantify Hg distribution between soil
113 carrier phases, in order to avoid cumulative errors intrinsic to SEPs. In addition, the
114 combination of X-ray diffraction (XRD) and chemical analysis allowed the
115 identification of the extracted phases and of possible overlaps between selective
116 extractions (cross recoveries). Intrinsic limitations of the selective extraction
117 procedure are discussed in the light of these results.

118 **2. Materials and methods.**

119 *2.1. Research areas*

120 The former gold mine flat is located in French Guiana (Fig. 1) on the Combat
121 Creek watershed (52°23'W, 4°35'N), a small catchment of ~1 km² covered by tropical
122 rain forest. Except for the two hilltops and for the lowland, the relief is characterized
123 by steep slopes (15-30%). The climate is tropical humid, with an annual average
124 rainfall of ~4000 mm (Barret, 2004).

125 The Combat Creek watershed is located on the 'Amina series' of the Guiana
126 Proterozoic shield consisting primarily of darkschist and thin sandstones (Milési et al.,
127 1995). Large gravel deposits from ancient rivers contain large amounts of gold,
128 resulting from the weathering of auriferous quartz veins from the Proterozoic shield
129 (Milési et al., 1995).

130 Soil distribution within the Combat Creek watershed is typical of French Guiana
131 and is related to soil position along the slopes (Boulet et al., 1979; Grimaldi et al.,
132 2001; Guedron et al., 2006). Ferralsols dominate upslope (Deckers et al., 1998),
133 having typically a high clay (< 2 µm size fraction) content and a micro-aggregated
134 structure extending over 1 m depth, which allows a good vertical water drainage
135 (Guehl, 1984). Ferruginous nodules are present throughout the entire ferralsol

profiles. Halfway down the slopes, ferralsols steadily evolves to acrisols, a massive alteritic horizon with a high content of fine silts at shallow depth (< 1 m). During rainfalls, a perched aquifer forms on the slope above this massive alteritic horizon. Following rainfalls, the aquifer is evacuated laterally, exporting preferentially clay-size particles and dissolution products (Molicova et al., 1997; Grimaldi et al., 2004). Downslope, the soils become hydromorphic, with dominant sands. A permanent aquifer is present and slowly drained by the river, thus imposing reducing conditions. Whatever the soil type, field observations have shown that quartz, kaolinite, and Fe-Al-(oxyhydr)oxides dominate mineralogy, quartz being the sole remnant from the primary rock-forming minerals. In the massive alteritic horizon, a few muscovite crystals were also observed. Soil pH ranged from 4.2 to 4.9. The upper part of the studied watershed (ferralsols and acrisols) was considered to be pristine based on the soil structure and texture.

In the lowland, ancient ‘Long Tom’ sluices and gold-bearing gravel heaps attest of former gold mining activities dated from the early 1950’s. These activities involved the removal of fine particles with water, in order to concentrate heavier gold-rich particles. Soils are thus strongly disorganized, and neither original structure nor texture is preserved. Present day soil granulometry reflects the former activity as gravels, sands and silts are dominant, while the clay-size fraction is almost absent. Hg droplets were also observed in these gold-mined gleysols during a prospective “panning” campaign. These soils can be described as disorganized gleysols according to their present geochemical characteristics.

158 *2.2. Sampling collection and analysis*

159 *2.2.1 Soil collection*

160 Three toposequences were sampled in the pristine part of the watershed, (i)
161 the first in the upper part of the basin, (ii) the second on the west (mountain) side and
162 (iii) the third next to the outlet of the basin (Fig. 1). Toposequences II and III reached
163 the gold-mined flats (profiles II-0 and III-0 in Fig. 1).

164 Thirteen profiles were collected in the former gold-mined flat. SL0 to SL9
165 profiles were mesh-sampled over a restricted 250 m² area in the flat zone (Fig. 1). G5
166 profile was sampled on a gravel heap. Soil profiles were sampled systematically
167 every 10 or 20 cm, down to 1-2 m depth, using an auger and collected in sterile
168 polyethylene bags.

169 *2.2.2 Soil conditioning, granulometry and chemical analysis*

170 Granulometry was determined with standard sieving and sedimentation
171 procedures (Avery and Bascomb, 1974; Rowell, 1994). Identification of the various
172 fractions was performed according to the Udden-Wentworth classification scheme
173 (Wentworth, 1922), and “gravel”, “sand”, “silt” and “clay” thus refer to particle
174 diameters (x) of $x > 2$ mm, $2\ \text{mm} < x < 50$ µm, $50\ \mu\text{m} < x < 2\ \mu\text{m}$ and $x < 2$ µm,
175 respectively. Total soil organic carbon ([C]), sulfur ([S]), and nitrogen ([N])
176 concentrations were determined from the dry combustion of soil sample aliquots
177 crushed and sieved to 63 µm, using a Fisons 1500CHNS auto-analyzer.

178 Soil samples aliquots used for Hg analysis, selective extractions and XRD
179 analysis were freeze-dried and sieved to $x < 2$ mm. This size fraction was
180 subsequently crushed to $x < 63$ µm. Ferruginous nodules were crushed also to x
181 < 63 µm and subsequently freeze-dried. Total Hg concentrations ([HgT]) were

182 determined by atomic absorption spectrophotometry after dry mineralization and gold
183 amalgamation with an automatic mercury analyzer (Altec, Model AMA 254). All
184 analyses were duplicated. The relative error was routinely ±5% and always
185 under ±10% (Roos-Barraclough et al., 2002). Detection limit (defined as three times
186 the standard deviation (SD) of the blank) is 0.005 μg g^{-1}. Concentrations obtained for
187 repeated analyses of certified reference materials (CRMs) never exceeded the
188 published range of concentration (0.090 ±0.012 μg g^{-1} and 0.091 ±0.008 μg g^{-1} for
189 CRMs 7002, and MESS-3, respectively). Total dissolved Hg concentration [$(HgT)_D$]
190 were analyzed by cold vapor atomic fluorescence spectrometry (CVAFS) after
191 conversion of all mercury species to Hg^0 (Bloom and Fitzgerald, 1988), using a
192 Tekran® instrument (Model 2500). Additional information on the method is available
193 elsewhere (Bloom and Fitzgerald, 1988). $(HgT)_D$ concentrations obtained for
194 repeated analyses of CRMs never exceeded the published range of concentration
195 (12.6 ±1.1 ng L^{-1} for ORMS-3). The detection limit is 0.05 ng L^{-1} (Bloom and
196 Fitzgerald, 1988).

197 Dissolved Fe and Al were determined by inductively coupled plasma-atomic
198 emission spectrometry (ICP-AES) using a Perkin-Elmer optima 3300DV. Calibration
199 was performed with using standard solutions for Fe and Al (Fluka® 44903 for Fe and
200 Fluka® 06155 for Al). Relative analytical errors were estimated for each sample from
201 triplicate measurements and were lower than 10%.

202 *2.3. Selective extraction procedure for Hg and major element analysis*

203 *2.3.1 Sample selection*

204 Along soil profiles, samples were selected on the basis of characteristics such
205 as granulometry, C and/or Hg contents, reflecting the textural and structural

206 variations along soil profiles. In pristine soils, the selection criteria were extreme
207 contents of C, Hg, clay-size fraction, and fine-silt fraction which increased in alterites.
208 In contaminated gleysols from the gold-mined flat, the selection relied mainly on the
209 abundance of the clay- and sand-size fractions, as well as on C and Hg
210 concentrations.

211 In addition to selected samples, selective extractions were performed for
212 quality assurance/quality controls (QA/QC) on 2 CRMs, namely a light sandy soil
213 (CRM 7002 - Czech Metrological Institute) and a marine sediment (MESS-3 -National
214 Research Council of Canada - Ottawa) and on two natural samples. The latter two
215 samples [acrisol I-1 (0-10 cm), and contaminated gleysol SL6 (30-50 cm)] were
216 chosen as models for the pristine and contaminated parts, respectively, of the
217 watershed. On all samples [HgT] was measured on both the supernatant and the
218 solid residue to assess extraction recovery. In addition, XRD data was systematically
219 collected on solid residues to identify dissolved mineral species.

220 *2.3.2 Selective extraction materials and procedure*

221 Four chemical extractions were chosen to selectively extract the main Hg
222 carrier phases reported in the literature for tropical soils: organic matter, amorphous
223 Fe oxides, and crystalline Fe/Al oxides.

224 For a given sample, selective extractions were performed on separate aliquots
225 of dry soil (~ 40 mg). All analytical procedures were conducted using ultra clean
226 sample handling to avoid laboratory contamination of low-level sample extracts and a
227 cross-contamination of high-level samples (Cossa and Gobeil, 2000). Specifically, all
228 materials in contact with the samples were previously acid washed (1 week in HNO_3
229 20%, 1 week in HCl 10%). All solutions were prepared from reagent grade chemicals
230 and supra-pure acids. Selective extractions were performed under a laminar hood in

8 ml Teflon® vessels at a 1:100 solid-to-liquid ratio (Bloom et al., 2003). At the end of the extraction time, samples were centrifuged to 3000 rpm for 20 min. The supernatant was analyzed for major elements. The solid residue was rinsed 3 times with 4 mL MilliQ® water to obtain a final volume of ~16 mL, which was subsequently freeze-dried before Hg analysis. The Hg content extracted by a given extraction was calculated as:

$$[Hg]_{extracted}\ (ng\ g^{-1}) = ([HgT] \times M_{sample} - M_{Hg\ in\ residue}) / M_{sample} \quad (1)$$

where M_{sample} is the mass of the aliquot used (in g) and $M_{Hg\ in\ residue}$ the mass of Hg measured in the residue (in ng).

To extract Hg bond to fulvic and humic compounds, a sample aliquot was digested in NH_4OH (1M) for 1h (Di Giulio and Ryan, 1987; Rodriguez Martin-Doimeadios et al., 2000; Veiga and Baker, 2004). Another extraction focused on organo-chelated Hg was performed by a 18h KOH digestion (1M) (Bloom et al., 2003). Extraction of Hg bond to amorphous Fe(III) oxide minerals and ferrihydrite was performed by adding ascorbate to a sample aliquot and allowing it to react at room temperature for 24h (Kostka and Luther III, 1994). Finally, extraction of Hg associated to all soil components except refractory minerals (i.e., silicates, primary minerals) was determined after the digestion of soil sample aliquot in a Suprapur HCl/HNO_3 solution (1/9 v/v ratio) for 10h at 70°C (Coquery et al., 1997; Bloom et al., 2003). All species associated to a specific extractant are labeled as follow: $(i)_j$ where i is the element and the subscribe j describes the extractant (i.e., $(i)_{NH4OH}$ for NH_4OH, $(i)_{KOH}$ for KOH, $(i)_{Asco}$ for ascorbate and $(i)_{HCl/HNO3}$ for HCl/HNO_3) and square brackets, $[i]_j$, are used for calculated concentrations (1). The concentration of Hg related to crystalline and refractory minerals (RC) is calculated as the difference between [HgT] and ascorbate plus NH_4OH extractions:

$$[Hg]_{RC}\ (ng\ g^{-1}) = (([HgT] \times M_{sample}) - M_{Hg\ Asco} - M_{Hg\ NH4OH}) / M_{sample} \quad (2)$$

This should be equivalent to a complete HF/HCl/HNO_3 extraction. Similar calculations were made to estimate the fraction of Hg bond to crystalline Fe and Al oxides ($[i]_{Cryst}$). For this purpose, concentrations obtained after HCl/HNO_3 extraction were considered as related to amorphous and crystalline Fe and Al oxides but not to refractory minerals. Thus, $[i]_{Cryst}$ was calculated as the difference between HCl/HNO_3 and ascorbate extraction :

$$[i]_{Cryst}\ (mg\ g^{-1}) = ([i]_{HCl/HNO3} \times M_{HCl/HNO3} - [i]_{Asco} \times M_{Asco}) / M_{sample} \quad (3)$$

A complementary pyrolysis procedure was used to assess the amount of Hg^0 present in the soils (Biester, 1994; Biester and Scholz, 1997; Bollen et al., 2008). After heating a ~1g sample aliquot for 48 hours at 180°C in a porcelain crucible, the content of Hg^0 was determined from the difference in Hg concentrations between raw and treated samples.

2.4. Physical methods

2.4.1 X-ray diffraction

X-ray diffraction (XRD) was performed on selected samples [Nodules I-2 (10-20 cm), I-1 (30-40 cm) and I-1 (180-200 cm)] for routine mineralogical identification, but also to identify the minerals targeted by the various selective extractions on CRM 7002, and MESS-3 standards, as well as on samples I-1 (0-10 cm) and SL6 (30-50 cm). For this purpose, XRD patterns were collected on solid residues of the different extractions, and compared to those obtained on the untreated samples.

XRD patterns were recorded on randomly oriented powders using a Bruker D5000 powder diffractometer equipped with a Si(Li) solid-state detector from Baltic Scientific Instruments and CuKα radiation (λ = 1.5418 Å). Intensities were recorded

from 5 to 80°2θ, using 0.04°2θ steps, and 40 s counting time per step. Measurements were duplicated on the CRM 7002 set of samples to ensure sampling homogeneity and selective extraction reproducibility (data not shown).

Mineralogical identification and unit-cell refinement

Basic data processing operations (e.g. background removal, diffractogram normalization) and mineralogical identification, based on peak positions and relative intensities, were performed using the Bruker Diffrac^{plus} EVA software and the ICDD database.

Relative intensities of XRD lines varied between raw and treated samples as the result of specific mineral dissolutions. To overcome the intensity variations due to the amount of measured sample, all XRD patterns were normalized to a selected quartz peak, as quartz was present in all samples and not dissolved by the reagents used. The peak used for normalization was selected so that (i) there is no peak overlap with other minerals and (ii) that its intensity is statistically meaningful. For iron oxides (hematite and goethite) present in Al-rich environments, experimental peak positions may differ significantly from theoretical ones as the result of isomorphic Al-for-Fe substitutions. In such case, theoretical unit-cell parameters of iron oxides were refined using the U-Fit program (Evain, 1992) to assess their Al-contents.

2.4.2 Micro X-ray fluorescence mapping and elemental analysis.

SL6 (30-50 cm) sample was freeze-dried, sieved to 300 µm and used for elemental mapping focused on Hg, Au, Al, Cl, Fe, Cr, Si, Ti, Mn, Ni, Ca and K. X-ray fluorescence yields (XRF) were measured with an Eagle III µ-XRF spectrometer (Röntgenanalytik Messtechnik GmbH) equipped with a Rh anode and a 40 µm poly-capillary. XRF was measured for 300 s per point over a 1.28×1.00 mm^2 surface area. The spectrometer was operated under vacuum at 25 kV and 500 µA so as to

maximize the fluorescence yield at the Hg L_α edge (9.99 keV) while keeping a statistically significant signal on light elements (down to Al K_α radiation - 1.49 keV). Further details on the method are given elsewhere (Doering et al., 2004).

2.5 Statistical treatment.

Since geochemical data were not normally distributed, the following parameters are reported: mean, standard error on the mean (SEM), median, 25th and 75th percentiles (25th perc. and 75th perc., respectively) and the number of observations (N - Webster, 2001). In addition, non parametric Mann-Whitney rank sum test (*U* test) and Kruskal-Wallis one way analysis of variance on ranks (*H* test) were used to compare two or more than two data sets, respectively. Pearson correlations were applied to compare multiple data set pairs. Correlation coefficient (CC) and P values (P) are reported.

3. Results

3.1 Blanks and CRMs

3.1.1 Mineralogy (QA/QC)

XRD patterns obtained on treated CRM samples indicate that halite was dissolved by all reagents (Supplementary data - Figs E1b. to E1e. and E2b to E2e). For CRM 7002, the chlorite component was partly dissolved by both NH_4OH and KOH. Exception made of halite, the effect of ascorbate was negligible. Most of the minerals identified by XRD were thus only affected by HCl/HNO_3: clinochlore, calcite and dolomite were totally dissolved, and an intensity decrease was observed for hornblende and, to a lesser extent, for kaolinite (Supplementary data – Figs E1e. and E2e.).

328 *3.1.2 Extraction recoveries (QA/QC)*

329 For NH_4OH, KOH and HCl/HNO_3 extractions, summation of M_{Hg} in both the
330 supernatant and the solid residue led to total Hg concentration consistent with those
331 of CRM 7002, MESS-3 and I-1 (10-20cm) sample. Relative error was routinely less
332 than ±10% (Tab. E1). Hg recovery was lower with ascorbate extraction, possibly due
333 to the loss of Hg^0 in the supernatant following Hg^{II} reduction (Battke et al., 2008).
334 Consistent with this hypothesis, additional measurements of $[(Hg)_D]$ in the
335 supernatant confirmed a steady decrease with time at the end of the extraction.

336 *3.2. Pristine soils*

337 *3.2.1 Granulometry, chemistry and mineralogy*

338 In the pristine area, the relative proportion of the clay-size fraction (< 2 µm)
339 decreased from ~90% in ferralsols to less than 30% in acrisols and gleysols (Fig. 2).
340 Ferruginous nodules made up most of the abundant gravel size fractions (x > 2 mm)
341 in ferralsols and acrisols, whereas for gleysols vegetal debris prevailed in this size
342 fraction. In the < 2 mm fraction, total C and S contents in superficial horizons
343 decreased from ferralsols and acrisols to gleysols while the C/N ratios were similar
344 for all soils, thus indicating an homogeneous mineralization of the fine organic matter
345 (OM - Bravard and Righi, 1991).

346 Minerals extracted by HCl/HNO_3 in sample I-1 (0-10cm) were identified as Al-
347 substituted iron oxides (goethite and hematite) and gibbsite (Fig. 3). Quartz, anatase,
348 kaolinite, and muscovite being essentially unaffected by the HCl/HNO_3 extraction
349 (Supplementary data – Fig. E3e.).

350 For HCl/HNO_3 and ascorbate extractions, Fe and Al concentrations were
351 correlated to the content of the clay size fraction (Tab. 1) showing that crystalline and

amorphous Fe and Al oxides were central in this fine fraction. Large Al and Fe concentrations were measured in supernatants following KOH, ascorbate and NH_4OH extractions. XRD confirmed that no crystalline Fe or Al oxides were dissolved by NH_4OH, thus supporting the dissolution of amorphous (or poorly crystalline) Fe and/or Al minerals. In addition, goethite was partially dissolved by ascorbate and hematite by KOH, as indicated by the ~10-20% intensity decrease of their characteristic XRD lines after these chemical extractions (Fig. 3). For all pristine soil samples, partial dissolution of these well-crystallized species is supported by the higher Al and Fe concentrations measured in KOH (median = 52.6% and 12.1% of $[Al]_{HCl/HNO3}$ and $[Fe]_{HCl/HNO3}$) and ascorbate (median = 24.7% and 21.7% of $[Al]_{HCl/HNO3}$ and $[Fe]_{HCl/HNO3}$) extracts compared to NH_4OH extracts (median=9.1% and 3.6% of $[Al]_{HCl/HNO3}$ and $[Fe]_{HCl/HNO3}$) (*H* test, $P < 0.001$).

$[Fe]_{HCl/HNO3}$, $[Al]_{HCl/HNO3}$, $[Fe]_{Asco}$ and $[Al]_{Asco}$ decreased steadily along the slopes from ferralsols to gleysols (Fig. 4), $[Fe]_{Asco}$ and $[Al]_{Asco}$ being commonly lower than $[Fe]_{Cryst}$ and $[Al]_{Cryst}$ for all profiles (Fig. 4). In ferralsols and acrisols, amorphous Fe and Al oxides were most abundant in the A horizon and in the top 50 cm of the B horizon, where weathering was most intense and granulometry dominated by clays. In the C horizon, the relative proportion of amorphous oxides decreased while well crystallized oxides and residual primary minerals became predominant, more especially in the fine silt size fraction. Al-for-Fe substitutions were identified in goethite (~33 Al mol%) and hematite (~10 Al mol%) from XRD unit-cell determinations and confirmed by the positive correlations between $[Fe]_{Cryst}$ and $[Al]_{Cryst}$ in B and C horizons (Fig. 4 - CC = 0.76; $P < 0.01$). Similar correlation was observed between $[Fe]_{Asco}$ and $[Al]_{Asco}$ (CC = 0.98; $P < 0.01$) for the whole profiles of pristine soils. The better correlation found between [Fe] and [Al] for ascorbate than

for crystalline oxide is suggestively due to an increase in [Al] related to Al extraction from gibbsite and in a lesser extent from kaolinite during HCl/HNO_3 extraction.

3.2.2 Hg in pristine soils

Total mercury concentrations measured in pristine soils matrix (0.01-0.49 $\mu g.g^{-1}$ - Fig. 2) were consistent with those recently reported for French Guiana soils (0.09-0.50 $\mu g.g^{-1}$ - Richard et al., 2000; Grimaldi et al., 2001; Guedron et al., 2006), the highest concentrations being measured in ferralsols. [HgT] decreased along the slope in acrisols and in gleysols (Fig. 2).

[HgT] were positively correlated with [Hg] extracted by HCl/HNO_3, KOH, NH_4OH and ascorbate (Tab. 1). In turn, [Hg] extracted by the four reagents were positively correlated to the content of the clay-size fraction, [S] and [C]. The clay-size fraction, which is composed of OM (S-groups) and Fe and Al minerals, thus represents the main Hg reservoir (Tab. 1).

In general, [Hg] extracted by all four reagents decreased with depth and from ferralsols to gleysols. However, Figure 5 shows that Hg extraction yields can be separated in two sets: (i) ferralsols and superficial acrisols and (ii) deep acrisol alteritic (C) horizons and gleysols. In both sets, NH_4OH extraction yields were significantly larger than ascorbate ones but followed the same trend. $(Hg)_{NH4OH}$ and $(Hg)_{Asco}$ extraction yields were highest in superficial horizons of both ferralsols and acrisols and steadily decreased with depth. Only in the upstream profiles I-1 and I-2 $(Hg)_{NH4OH}$ and $(Hg)_{Asco}$ extraction yields were constant with depth. In gleysols and deep alteritic horizons of acrisols, both $(Hg)_{NH4OH}$ and $(Hg)_{Asco}$ decreased rapidly with depth, whereas $(Hg)_{RC}$ extraction yields increased strongly with increasing depth. $(Hg)_{RC}$ decreased with increasing depth in the B horizons of ferralsols and acrisols, then increasing steadily in the ferralsol C horizons. $(Hg)_{KOH}$ extraction yields were

highly variable with highest values in ferralsol and acrisol B horizons. In pristine gleysols (profile II-1), $(Hg)_{KOH}$ extraction yields increased with increasing depth over the first 50 cm, while decreasing in the C horizon.

3.3 Ferruginous nodules in pristine soils

3.3.1 Chemistry and mineralogy

Ferruginous nodules (> 2 mm) were abundant (mean ±RSD = 45.8 ±28.6% total weight), especially in superficial horizons of the pristine toposequences, their relative abundance decreasing from ferralsols to gleysols. Nodules from samples I-2 (10-20 cm), I-2 (30-40 cm) and I-2 (180-200 cm) contained quartz, Al-substituted hematite and goethite, gibbsite and kaolinite. Figure 6 shows the steady increase of muscovite (Mu), paragonite (Pa), gibbsite (Gb) and rutile (Ru) contents from surface (sample I-2, 10-20 cm) to depth (sample I-2, 180-200 cm - Fig E4). This mineralogical evolution is consistent with chemical data as $[Fe]_{HCl/HNO3}$ and $[Al]_{HCl/HNO3}$ steadily decreased with increasing depth.

Position of the iron oxide peaks (goethite and hematite) shifted to lower angular values with increasing depth (Fig. 6, inset), thus indicating the lengthening of unit-cell parameters, and thus the probable decrease of Al-for-Fe substitution, since the ionic radius of Al is smaller than Fe (Shannon, 1976). The extent of this substitution was assessed for the two oxides by refinement of the unit-cell parameters and empirical relations between the Al content and the lattice parameters (Schulze, 1984; Stanjek and Schwertmann, 1992). Al substitutions in hematite decreased from 17 mol% (surface) to 10 mol% (deep alteritic horizons) and were almost constant (~20 mol%) over the entire profile for goethite. Uncertainty on lattice parameters (and therefore on Al substitution quantification) was low for hematite

owing to the sharp and numerous diffraction peaks, but higher for goethite. Indeed, few isolated diffraction peaks were available for the determination of the unit-cell parameters and peaks were broadened.

The intensity of hematite diffraction lines increased with decreasing depth, thus indicative of a higher proportion of hematite towards the surface, consistent with its status of final alteration product of iron-rich phases (Schwertmann and Latham, 1986). Hematite and goethite are indeed the most thermodynamic stable iron oxides in surface conditions. Amorphous oxides were present as minor constituents since Al and Fe extracted by ascorbate and NH_4OH never exceeded 7% of their HCl/HNO_3 counterparts (Fig. E5). As in pristine soils matrix, KOH extraction likely induced the partial dissolution of gibbsite as $[Al]_{KOH}$ was large (median = 51.5% of $[Al]_{HCl/HNO3}$).

3.3.2 Hg in ferruginous nodules of pristine soils

For surface horizons, [HgT] were much lower in nodules than in the soil matrix. [HgT] increased with increasing depth, similar values being obtained for nodules and soil matrix in the deepest sample of acrisol I-1 profile. [HgT] were even larger in nodules than in soil matrix for ferralsol I-2 samples below 50 cm depth (Fig. E5).

[HgT] was positively correlated with $[Hg]_{HCl/HNO3}$ and $[Hg]_{KOH}$ ($P < 0.05$) and with $[Fe]_{HCl/HNO3}$ and $[Al]_{HCl/HNO3}$ ($P < 0.05$). $(Hg)_{HCl/HNO3}$ extraction yields were larger in ferralsol nodules from deep horizons compared to surface ones. Conversely, in acrisols they were larger for surface horizons. For all nodules these yields scattered about 80%. $(Hg)_{Asco}$ and $(Hg)_{NH4OH}$ extraction yields rarely exceeded 10% and rapidly decreased with increasing depth in both acrisols and ferralsols. $(Hg)_{KOH}$ (44.8 ±30.2%) extractions yields were systematically larger than the sum $(Hg)_{Asco}$ + $(Hg)_{NH4OH}$, and progressively decreased downwards in I-1 and I-2 profiles.

3.4 Contaminated gold-mined soils

3.4.1 Granulometry, mineralogy and chemistry

In the gold-mined flat, contaminated gleysols contained a large proportion of gravel size fractions (mainly quartz gravels and stones, mean ± RSD = 42.7 ±24.6% total weight) and the < 2 mm fraction was dominated by sands in contrast with pristine soils (Fig. 2b). Total organic C largely exceeded the concentrations determined in pristine soils and elevated C/N ratios were characteristic of poorly mineralized OM (data not shown). Leaves and wood debris were visible in the litter.

Minerals present in sample SL6 after HCl/HNO_3 extraction were quartz, kaolinite, muscovite, diaspore, rutile and microcline. Gibbsite was for the most part dissolved by HCl/HNO_3, which also possibly partially dissolved kaolinite. The absence of Fe oxides is consistent with the low $[Fe]_{HCl/HNO3}$ values (0.35 $mg.g^{-1}$).

Amorphous and crystalline Fe and Al oxides were scarce in contaminated soils as shown by the low Al and Fe concentrations extracted by any reagent compared to pristine soils. For all soil profiles, $[Al]_{HCl/HNO3}$ and $[Fe]_{HCl/HNO3}$ were maximum in surface horizons, and sharply decreased to ~5 $mg.g^{-1}$ at ~40 cm depth, except for II-0, SL0 and G5 profiles.

As for pristine soils, partial gibbsite dissolution by KOH was evidenced by chemistry data as $[Al]_{KOH}$ (median = 76.3% of $[Al]_{HCl/HNO3}$) were larger than $[Al]_{Asco}$ (median = 55.7% of $[Al]_{HCl/HNO3}$) and $[Al]_{NH4OH}$ (median = 28.5% of $[Al]_{HCl/HNO3}$) (*U* test, $P < 0.05$). Fe oxides were also more attacked by ascorbate ($[Fe]_{Asco}$ median = 31.1% of $[Fe]_{HCl/HNO3}$) than by KOH and NH_4OH ($[Fe]_{KOH}$: median = 17.3% of $[Fe]_{HCl/HNO3}$ and $[Fe]_{NH4OH}$: median = 14.8% of $[Fe]_{HCl/HNO3}$).

3.4.2 Hg in contaminated gold mined soils

[HgT] values measured in gleysols from the gold-mined flat (up to ~10 $\mu g.g^{-1}$ in SL6 profile) were up to 5 times higher than those determined in gleysols from the pristine area (Fig. 2b). Although extremely variable, even over very short distances, these values were consistent with those determined in Hg-contaminated soils from different gold-mining regions (Lechler et al., 1997; Lechler et al., 2000; Richard et al., 2000; Sladek and Gustin, 2003), and positively correlated with [Hg] extracted by all four reagents (Tab. 2a and 2b). Contrarily to the pristine area, where gleysols were the pole of lowest [HgT], the only significant correlation of [HgT] with other soil parameters was observed with the sand-size fraction ($P < 0.05$).

μ-XRF map (Fig. 7) shows that Hg was not homogeneously distributed in sample SL6 (30-50cm). Indeed, Hg is essentially present as “hot-spots” of 30 to 100 μm in diameter. In these hot-spots, Hg concentration is not correlated with any element (data not shown), except for a covariation with Au (Fig. 7). These spots are thus likely Hg^0 droplets, possibly amalgamated with Au. Consistently, pyrolysis measurements showed that almost 60% of total Hg was desorbed at 180°C. However, lower percentages of desorbed Hg were determined for SL8 and SL7 samples, thus suggesting that Hg^0 was not systematically the main Hg form over the entire former gold-mined flat (Fig. 8). Consistently, selective extractions have shown that Hg was partially associated to OM and amorphous oxides for some samples as shown by the NH_4OH and ascorbate extraction yields. Such associations remained however minor as $(Hg)_{NH4OH}$ (median = 28.4%) and $(Hg)_{Asco}$ (median = 14.7%) extraction yields only seldom exceeded 50 and 30%, respectively (Fig. 8). Relative proportion of Hg associated to refractory minerals was negligible as $(Hg)_{HCl/HNO3}$ extraction yields were systematically ~100%. In this case, large $(Hg)_{RC}$ reflect the

498 proportion related to Hg^0 (Fig.8). KOH extraction yields also were high (median =
499 86.5%), being always higher than 80% in the uppermost 40 cm.

500 **4. Discussion**

501 *4.1 Selective extractions*

502 Further investigation was performed to unravel the reactions leading to Hg
503 reduction and loss during ascorbate extraction, although $[Hg]_{Asco}$ were not biased,
504 being calculated from the analysis of the solid residue. Results of the pyrolysis
505 procedure were also questionable as the pyrolysis (180°C) of marine sediment
506 MESS-3 has shown no significant desorption of Hg, while almost 70% of total Hg
507 desorbed from light sandy soil CRM 7002 under the same conditions. It is thus likely
508 that in addition to Hg^0, Hg bond to OM was partially desorbed during pyrolysis.
509 Pyrolysis temperature (180°C) was indeed close to the temperature range reported
510 by Biester and Scholz (1997) for the thermal release of Hg bound to organic
511 compounds (200-350°C). This is especially relevant for the assessment of the
512 different Hg-compartments in organic-rich contaminated soils.

513 Cross recoveries between selective extractions were observed for both CRMs
514 and natural samples, but it was also possible to attribute selective mineral extractions
515 to each reagent. The selective character of a given extraction depends on the
516 considered soil matrix, as reagent selectivity depends both on the nature of
517 components present and on their reactivity with respect to a given reagent.
518 Overlapping extractions further increase the uncertainty on the relative proportion of
519 Hg associated to any carrier phase. Although chemical data may help to assess
520 cross recoveries, the restricted and variable selectivity of the different reagents
521 precludes the use of selective extractions as standardized procedures for

environmental studies. Specifically, the use of selective extractions needs preliminary investigation to assess reagent selectivity for a given soil matrix.

4.2 Hg distribution in pristine soils

The study of Hg distribution in a soil has to take into account the original soil cover formation, its current evolution and its present topographic position, that is its position in the soil association (Fritsch et al., 2006). These factors are indeed responsible, at least partially, for the relative abundance and the reactivity of soil organic and mineral components, including Hg carriers, thus providing additional insight in the Hg natural equilibrium and contents.

4.2.1 Hg carrier phases in soil profiles

A positive correlation between the relative amount of the clay-size fraction and C, S, [Fe] and [Al] extracted by HCl/HNO_3, NH_4OH and ascorbate is shown in Table 2. Hg is thus likely associated with finely divided Fe and Al organic complexes and/or with organic coatings on Fe/Al oxides. Several authors have already shown that in Amazonian micro-aggregated horizons, micropeds develop from the bonding between clays, organic matter and iron oxides through the formation of carbon-coatings on mineral surfaces (Tandy et al., 1990; Malengreau and Sposito, 1997; Do Nascimento et al., 2004).

Specific bonding of Hg with sulfur groups from finely divided organic matter may be inferred from the above described correlations for all pristine soils. This is consistent with previous reports of organics, and more especially of reduced sulfur groups, being the most effective sorbents for Hg in acidic environments (pH < ~4.5-5.0), compared to iron oxides and clay minerals (Andersson, 1979; Schuster, 1991; Roulet and Lucotte, 1995; Skyllberg et al., 2000; Skyllberg et al., 2006; Manceau and

546 Nagy, 2008).

547 In addition to this essential organic contribution, Hg contents in soils from
548 French Guiana are also controlled by the actual nature of Fe and Al (oxyhydr)oxides
549 (Roulet and Lucotte, 1995; Roulet et al., 1998). In pristine soil matrix, large $[Hg]_{Asco}$
550 and $[Hg]_{HCl/HNO3}$ values were indeed attributed to Al-substituted amorphous and
551 crystalline Fe oxides. As a result of their larger surface areas compared to their
552 crystalline counterparts, amorphous or poorly crystalline species have an increased
553 adsorption capacity, (Schwertmann and Latham, 1986; Schwertmann and Cornell,
554 2000). The positive correlation between $[Hg]_{KOH}$ and $[Al]_{KOH}$ supports also the
555 importance of Al oxides as a reservoir for Hg. This reservoir is accessible through
556 KOH and, to a lesser extent, through ascorbate extractions, thus the large $[Al]_{Asco}$
557 plead for the partial dissolution of (amorphous) Al (oxyhydr)oxides (Schwertmann
558 and Latham, 1986).

559 In nodules, as in soil matrix, Hg is bond to Al and Fe oxides. Ferruginous
560 nodules are abundant in ferralsols and acrisols, where they represent ~50% of total
561 soil materials and thus represent large Hg reservoirs, [HgT] being similar in nodules
562 and soil matrix. In addition to Al-substituted hematite and goethite, gibbsite
563 contributes significantly to Hg retention in soil nodules, especially in surface horizons,
564 as suggested by the large $(Hg)_{KOH}$ extraction yields associated with large $[Al]_{KOH}$
565 values. This observation is consistent with the strong affinity of Hg(II) for gibbsite
566 (Kim et al., 2004a; Kim et al., 2004b; Weerasooriya et al., 2007).

567 Finally, the contribution of refractory minerals (identified as muscovite,
568 anatase, rutile and kaolinite) is non negligible, although minor, in pristine soils as the
569 median $(Hg)_{HCl/HNO3}$ extraction yield is only 89.8%.

570 *4.2.2 Influence of soil structure on Hg distribution in soil profiles*

571 From the above description, it appears that the vertical distribution of OM,
572 Al/Fe (oxyhydr)oxides and ferruginous nodules in the soil matrix rules Hg distribution.
573 In the following section, pedological and chemical characteristics responsible for the
574 spatial distribution of these components in soil profiles will be discussed.

575 Upslope, large [HgT] have been measured in the matrix of the ferralsol micro-
576 aggregated horizons (i.e., A and B horizons). The micro-aggregated structure confers
577 a good water drainage capacity to ferralsols, favoring water flow and oxidizing
578 conditions. As a result, Hg is spread throughout these micro-aggregated horizons as
579 the result of both significant leaching and migration of atmospheric inputs (Guedron
580 et al., 2006). Plant litter is rapidly mineralized in surface horizons, and the rapid
581 turnover of humic substances leads to the migration of fulvic acids in deeper organo-
582 mineral horizons where they are complexed to Fe and Al oxides (Roulet and Lucotte,
583 1995). Thus, Hg originating from plant litter decomposition and/or from atmospheric
584 fallouts can migrate into the organo-mineral horizons as organic-Hg complexes and
585 progressively adsorb onto Al/Fe (oxyhydr)oxides. Soil ecosystem engineers (soil
586 invertebrates and roots) also play an important role in the particulate transfer of Hg
587 by enhancing aggregation (Velasquez et al., 2007) and soil hydraulic conductivity
588 (Grimaldi et al., 2008) through biogenic soil organization. In the micro-aggregated B
589 horizon of ferralsols, the distribution of amorphous Fe oxides is positively correlated
590 to [HgT], although their relative abundance is lower than or similar to that of the
591 crystalline varieties. The comparison of $[Fe]_{Cryst}$ and $[Fe]_{Asco}$ indicates that the relative
592 proportion of crystalline Fe oxides is increased further in the superficial layer and in
593 the deep alteritic horizons compared to the micro-aggregated B horizon of ferralsols.
594 In addition, the positive correlations between $[Hg]_{RC}$ and $[Fe]_{Cryst}$ or $[Al]_{Cryst}$

595 throughout the entire soil profile suggest that $[Hg]_{RC}$ is partially associated to Al-
596 substituted crystalline Fe oxides. In this case, the sum of [Hg] adsorbed onto
597 amorphous and crystalline Fe oxides would be comparable or larger than the part
598 related to organic compounds.

599 The micro-aggregated structure of ferralsols disappears progressively with
600 increasing depth, giving rise to deep mineral horizons with a continuous structure
601 composed of large mineral relics. Parental material relics “dilute” Al/Fe oxides and
602 thus reduce the overall sorption capacity of deep horizons. Another essential factor is
603 the lower permeability of deep horizons which limits the downward migration of Hg
604 (Guedron et al., 2006). Hg content thus mainly results from rock weathering and
605 pedogenesis (Guedron et al., 2006), [HgT] being mainly associated with coarse-
606 grained goethite and hematite.

607 In ferralsol nodules, Hg is mainly bond to Al-substituted hematite and goethite,
608 and to gibbsite. As in ferralsol matrix, highest [HgT] values were measured in the
609 micro-aggregated horizon. Indeed, the downward decrease of $(Hg)_{HCl/HNO3}$ extraction
610 yields and the mineralogical evolution suggest that A and B horizons nodules are
611 primarily composed of neo-formed minerals, thus indicating an advanced stage of
612 pedogenesis and weathering in superficial horizons. Mineral neoformation also
613 appears to favor the incorporation of atmospheric Hg inputs.

614 Halfway down the slope, in acrisols, a similar mineralogical and structural
615 contrast is observed between superficial (A and B horizons) and alteritic horizons.
616 This transition is sharp as evidenced by the increase of the silt fraction and by the
617 decrease of [HgT]. As for ferralsol, the increase of refractory minerals with increasing
618 depth is most likely responsible for the observed decrease of [HgT].

Downslope, in gleysols, [HgT] were lower since fine organic fraction, S and amorphous oxides are less abundant than upslope, even though carrier phases were similar to those identified in ferralsols and acrisols. Gleysols are depleted in iron oxides and the main minerals are kaolinite, gibbsite, muscovite and quartz. Hg extracted by NH_4OH never exceeds 40% of [HgT] in gleysol surface horizons and rapidly decreases with depth. Hg bond to amorphous oxides never exceeds 20% of [HgT], and almost 50% of [HgT] is likely associated to Al-substituted crystalline Fe oxides, gibbsite and to refractory minerals. Consistently, Hg, Fe, and Al extracted by HCl/HNO_3 are together positively correlated in the gleysol profile. In depth, Hg is less abundant and mainly associated to refractory minerals since $(Hg)_{RC}$ extraction yields increase with increasing depth.

4.2.3 Influence of soil formation on the distribution of Hg over the soil association

The soil association results from the ferralsols current imbalance, which leads to temporal and spatial evolutions (Boulet et al., 1993; Grimaldi et al., 2004). Because of their major role as Hg reservoirs, the following description of Hg distribution along the toposequence will thus focus on OM and Fe oxides behavior in the soil association.

In organic horizons, the [HgT] decrease along the slopes correlates with the decrease of their C and S contents. However, organic horizons in gleysols are characterized by an increased proportion of OM in gravel size fractions (> 2 mm) and thus by a lower degree of mineralization of coarse OM because of hydromorphy. Consequently, the overall reactivity of coarse OM towards Hg (including the reactivity of S groups) decreases when all soil fractions are considered even if C and S remain abundant (Andersson, 1979; Kerndorff and Schnitzer, 1980; Schnitzer and Kerndorff, 1981; Ochs et al., 1994; Gasper et al., 2007).

644 The decreasing proportion of Fe and Al (oxyhydr)oxides down the slope
645 results from the combined effect of diffuse erosion and leaching due to the lateral
646 drainage of horizons overlying the alteritic horizons of acrisols and of the progressive
647 occurrence of hydromorphy (Boulet et al., 1979; Fritsch et al., 1986; Fritsch et al.,
648 2006; Grimaldi et al., 2004; Lucas et al., 1996). Drainage induces a texture
649 coarsening from the original clayey texture of ferralsols to the sandy-loam texture of
650 gleysols, whereas hydromorphy induces the dissolution of crystalline and amorphous
651 Al-bearing Fe oxides and the export of the reduction products through the
652 hydrographic network (Grimaldi et al., 2008). Both processes result in the relative
653 increase of coarse fractions composed mainly of quartz and neoformed kaolinite
654 (Boulet, 1978; Roulet et al., 1998) which possess a low affinity for Hg (Sarkar et al.,
655 1999; Sarkar et al., 2000).

656 *4.3 Influence of former gold mining activities on anthropogenic Hg pool in soils*

657 In contrast to pristine soils, Hg appears to be associated mainly with the
658 prevailing sandy fraction. In highly contaminated sites Hg has been identified as Hg^0,
659 insoluble cinnabar and metacinnabar (Lechler et al., 1997; Slowey et al., 2005;
660 Slowey and Brown, 2007). In the present study, mercury sulfides (cinnabar and
661 metacinnabar) are most likely insignificant as no positive correlation was found
662 between Hg and S. $(Hg)_{HCl/HNO3}$ extraction yields are systematically close to 100%
663 and support further the low amount of mercury sulfides which are essentially
664 insoluble in concentrated HCl/HNO_3 (Mikac et al., 2002; Mikac et al., 2003)..

665 The probable presence of Hg^0 is supported by the observation of macroscopic
666 Hg^0 droplets during a prospective “panning” in the sandy horizon of gold-mined
667 gleysols (50-100 cm depth) next to profile III-0. It was however impossible to assess

668 the distribution of the Hg^0 droplets along vertical profiles. μXRF confirmed the
669 presence of isolated Hg^0 droplets (~100 μm in diameter) in sample SL6 (30-50cm),
670 possibly amalgamated with micrometric gold particles. Consistently, pyrolysis
671 measurements have shown that Hg^0 generally prevail in the former gold-mined flat
672 soils, with some exceptions (e.g., SL7 and SL8 profiles). In the latter profiles, the
673 reduced contribution of Hg^0 can result from its oxidation, known to be fast in tropical
674 environments (Dominique et al., 2007). If geochemical conditions are not
675 permanently reducing, as in the surface horizons, Hg^0 can be oxidized, allowing
676 adsorption onto OM and minerals. The relative proportion of Hg bond to OM is
677 however lower than in pristine soils, $(Hg)_{NH4OH}$ extraction yields rarely exceeding
678 50%. As previously discussed, the overall limited mineralization of OM is most likely
679 responsible for the low reactivity of OM for Hg. Similarly, the relative proportion of Hg
680 bond to amorphous Fe oxides is low (up to 15%), these oxides being scarce in
681 hydromorphic environments. Finally, the part related to refractory minerals (i.e.,
682 quartz, kaolinite and muscovite) appears to be negligible since $(Hg)_{HCl/HNO3}$ extraction
683 yields are always close to 100%.

684 **5. Conclusion**

685 The combination of selective extractions with physical techniques (XRD and
686 μXRF) significantly improved the determination of Hg speciation by allowing the
687 identification of Hg carrier phases targeted by the different extractants. However, the
688 quantification of Hg associated to a given carrier phase is affected by intrinsic bias,
689 especially because of probable overlaps between the different extraction procedures.
690 Thus, selective extractions can not be used as a standard procedure for natural

691 samples since the use of selective extractions requires the preliminary assessment of
692 reagent selectivity for a given soil matrix.

693 By coupling XRD and selective extractions, the main Hg carrier phases in
694 pristine soils were identified as sulfur groups from organic matter, amorphous and
695 crystalline Al-substituted Fe oxides and, to a lower extent, Al oxides. The relative
696 contribution of these carriers to the overall Hg concentration was dependent on their
697 relative abundance which is controlled by the pedogenetic evolution along the slopes,
698 and more especially by redox conditions, hydric properties, and ecosystem
699 engineers. In the former gold-mined flat, Hg was found mainly as Hg^0, possibly
700 amalgamated with Au, and as oxidized Hg^{II} associated with organic matter, Fe and/or
701 Al oxides in surface horizons.

702 *5.1 Concluding Remarks*

703 These findings have major implications on the contamination of hydrosystems
704 in tropical regions, where soil erosion due to deforestation, gold mining and
705 agricultural processes are intense and lead to the release of Hg-rich clay-size
706 particles as shown by the low proportion of clay-size fractions in gold-mined gleysols.
707 When entering suboxic and anoxic environments (e.g. river or dam sediments), Hg
708 bond to clay-size particles indeed becomes accessible to ferri- and sulfato-reducing
709 bacteria that are the main factors of Hg methylation (Fitzgerald and Lamborg, 2003;
710 Fleming et al., 2006). Hg bound to OM and Fe oxides is specifically concerned as
711 these major components of the clay-size fraction are essential nutriments for
712 methylating micro-organisms and final electron acceptors of their metabolism. In
713 addition, former gold mined soils are potential important sources of Hg for
714 methylating bacteria. Indeed, Dominique et al. (2007) have shown that anthropogenic

715 Hg^0 from former gold-mining activities also promotes the production of MMHg in the
716 Amazonian hydrosystems and its availability to trophic webs.

717 **Acknowledgments**

718 This research was supported mainly by the CNRS through its “Mercury in
719 French Guiana” research program and by the Boulanger Mine Company (CMB –
720 Cayenne) through a Ph.D. granted to Stéphane Guédron. The authors thank Manuel
721 Munoz and Mathieu Corazzi (LGCA – Grenoble) for the assistance with μXRF
722 mapping, Vincent Perrot and Nicolas Geoffroy (LGIT – Grenoble) for technical
723 support during the project, and Max Sarrazin (IRD – Cayenne) who performed soil
724 granulometry and C, N and S analyses.

725 **References**

726 Andersson, A., 1979. Mercury in soils. In: J.O. Nriagu (Editor), The biogeochemistry
727 of mercury in the environment. Elsevier, Amsterdam, pp. 80-111.
728 Avery, B.W. and Bascomb, C.L., 1974. Soil survey laboratory methods. Technical
729 Monograph, 6. Soil Survey of England and Wales, Harpenden.
730 Barbosa, A.C., Souza, J.D., Dorea, J.G., Jardim, W.F. and Fadini, P.S., 2003.
731 Mercury Biomagnification in a Tropical Black Water, Rio Negro, Brazil. Arch.
732 Environ. Contam. Toxicol. 45(2): 235-246.
733 Barret, J., 2004. Illustrated Atlas of French Guyana. French Guyana Publications,
734 Cayenne, 219 pp (in French).
735 Battke, F., Ernst, D., Fleischmann, F. and Halbach, S., 2008. Phytoreduction and
736 volatilization of mercury by ascorbate in Arabidopsis thaliana, European beech
737 and Norway spruce. Appl. Geochem. 23(3): 494-502.

738 Beldowski, J. and Pempkowiak, J., 2003. Horizontal and vertical variabilities of
739 mercury concentration and speciation in sediments of the Gdansk Basin,
740 Southern Baltic Sea. Chemosphere. 52: 645-654.
741 Beldowski, J. and Pempkowiak, J., 2007. Mercury transformations in marine coastal
742 sediments as derived from mercury concentration and speciation changes
743 along source/sink transport pathway (Southern Baltic). Estuarine Coastal Shelf
744 Sci. 72(1-2): 370-378.
745 Benoit, J.M., Gilmour, C.C., Heyes, A., Mason, R.P. and Miller, C.L., 2003.
746 Geochemical and biological controls over methylmercury production and
747 degradation in aquatic ecosystems. In: Y. Cai and O.C. Braids (Editors),
748 Biogeochemistry of Environmentally Important Trace Elements. Oxford
749 University Press, pp. 262-297.
750 Biester, H., 1994. Moglichkeiten der anwendung eines temperaturgesteuerten
751 pyrolyseverfahrens zur bestimmung der bindungsform des quecksilbers in
752 boden und sedimenten. Heidelberger Geowiss. Abh. 75, 156 pp.
753 Biester, H. and Scholz, C., 1997. Determination of mercury binding forms in
754 contaminated soils: Mercury pyrolysis versus sequential extractions. Environ.
755 Sci. Technol. 31: 233-239 (in German).
756 Bloom, N.S. and Fitzgerald, W.F., 1988. Determination of volatil mercury species at
757 the picogram level by low-temperature gas chromatography with cold-vapor
758 atomic fluorescence detection. Anal. Chim. Acta. 208: 151-161.
759 Bloom, N.S., Preus, E., Katon, J. and Hiltner, M., 2003. Selective extractions to
760 assess the biogeochemically relevant fractionation of inorganic mercury in
761 sediments and soils. Anal. Chim. Acta. 479: 233-248.

762 Bollen, A., Wenke, A. and Biester, H., 2008. Mercury speciation analyses in $HgCl_2$-
763 contaminated soils and groundwater - Implications for risk assessment and
764 remediation strategies. Water Res. 42(1-2): 91-100.
765 Boszke, L., Kowalski, A., SzczuciÅ„ski, W., Rachlewicz, G., Lorenc, S.A. and Siepak,
766 J., 2006. Assessment of mercury mobility and bioavailability by fractionation
767 method in sediments from coastal zone inundated by the 26 December 2004
768 tsunami in Thailand. Environ. Geol. 51(4): 527-536.
769 Boulet, R., 1978. Existence of high lateral differentiation systems in French Guiana's
770 ferrallitic soils: a new example of an imbalanced pedological cover. Soil Sci. 2:
771 75-82 (in French).
772 Boulet, R., Grugiere, J.M. and Humbel, F.X., 1979. Relationships between soil
773 organization and water dynamics of septentrional French Guiana. Agronomic
774 consequences of an evolution controlled by a mainly tectonic desequilibrium.
775 Soil Sci. 1: 3-18 (in French).
776 Boulet, R., Lucas, Y., Fritsch, E. and Paquet, H., 1993. Landscape geochemistry:
777 role of soil cover. In: French. Acad. Sci. (Editor), Sedimentology and surface
778 geochemistry, Paris, pp. 55-76 (in French).
779 Brabo, E.S., Angelica, R.S., Silva, A.P., Faial, K.R.F., Mascarenhas, A.F.S., Santos,
780 E.C.O., Jesus, I.M. and Loureiro, E.C.B., 2003. Assessment of mercury levels
781 in soils, waters, bottom sediments and fishes of the Acre state in brazilian
782 amazon. Water Air Soil poll. 147: 61-77.
783 Bravard, S. and Righi, D., 1991. Characterization of fulvic and humic acids from an
784 oxisol-spodosol toposequence of Amazonia, Brazil. Geoderma. 48(1-2): 151-
785 162.

786 Carmouze, J.P., Lucotte, M. and Boudou, A., 2001. Le Mercure en Amazonie Rôle
787 de l'homme et de l'environnement, Risques sanitaires. IRD Editions, Bondy,
788 494 pp (in French).
789 Charlet, L. and Sposito, G., 1987. Monovalent ion adsorption by an oxisol. Soil Sci.
790 Soc. Am. J. 51: 1155-1160.
791 Charlet, L. and Sposito, G., 1989. Bivalent ion adsorption by an Oxisol. Soil Sci. Soc.
792 Am. J. 53(5): 691-695.
793 Coquery, M., Cossa, D. and Sanjuan, J., 1997. Speciation and sorption of mercury in
794 two macro-tidal estuaries. Marine Chem. 58(1-2): 213-227.
795 Coquery, M., Cossa, D., Azemard, S., Peretyazhko, T. and Charlet, L., 2003.
796 Methylmercury formation in the anoxic waters of the Petit-Saut reservoir
797 (French Guiana) and its spreading in the adjacent Sinnamary river. J. Phys.
798 IV. 107: 327-331.
799 Cossa, D. and Gobeil, C., 2000. Mercury speciation in the Lower St. Lawrence
800 estuary. Can. J. Fish. Aquat. Sci. 57: 138-147.
801 De Oliveira, S.M.B., Melfi, A.J., Fostier, A.H., Forti, M.C., Favaro, D.I.T. and Boulet,
802 R., 2001. Soils as an important sink for mercury in the Amazon. Water Air Soil
803 Poll. 26: 321-337.
804 Deckers, J., Nachtergaele, F. and Spaargaren, O., 1998. World reference base for
805 soil resources. ACCO Publishers, 165 pp.
806 Di Giulio, R.T. and Ryan, E.A., 1987. Mercury in soils, and clams from a North
807 Carolina peatland. Water, Air and soil poll. 33: 205–219.
808 Do Nascimento, N.R., Bueno, G.T., Fritsch, E., Herbillon, A.J., Allard, T., Melfi, A.J.,
809 Astolfo, R., Boucher, H. and Li, Y., 2004. Podzolization as a deferralitization

process: a study of an Acrisol-Podzol sequence derived from Palaeozoic sandstones in the northern upper Amazon Basin. Eur. J. Soil Sci. 55: 523-538.

Do Valle, C.M., Santana, G.P., Augusti, R., Egreja Filho, F.B. and Windmoller, C.C., 2005. Speciation and quantification of mercury in Oxisol, Ultisol, and Spodosol from Amazon (Manaus, Brazil). Chemosphere. 58(6): 779-792.

Doering, E.R., Havrilla, G.J. and Miller, T.C., 2004. Disilicide Diffusion Coating Inspection by Micro X-Ray Fluorescence Imaging. J. Nondestr. Eval., 23(3): 95-105.

Dominique, Y., Muresan, B., Duran, R., Richard, S. and Boudou, A., 2007. Simulation of the Chemical Fate and Bioavailability of Liquid Elemental Mercury Drops from Gold Mining in Amazonian Freshwater Systems. Environ. Sci. Tech. 41(21): 7322 -7329.

Eagenhouse, R.P., Young, D.R. and Johnson, J.N., 1978. Geochemistry of mercury in Palos Verdes sediments. Environ. Sci. Technol. 12: 1151–1157.

Evain, M., 1992. U-FIT: A Cell Parameter Refinement Program. IMN Nantes.

Fitzgerald, W.F. and Lamborg, C.H., 2003. Geochemistry of mercury in the environment. In: B. Sherwood Lollar (Editor), Treatise on Geochemistry. Elsevier, pp. 107-148.

Fleming, E.J., Mack, E.E., Green, P.G. and Douglas, C.N., 2006. Mercury methylation from unexpected sources: molybdate-inhibited freshwater sediments and iron-reducing bacterium. Appl. Environ. Microbiol. 72(1): 457-464.

Fontes, M.P.F. and Gomes, P.C., 2003. Simultaneous competitive adsorption of heavy metals by the mineral matrix of tropical soils. Appl. Geochem. 18(6): 795-804.

835 Frery, N., Maury-Brachet, R., Maillot, E., Deheeger, M., Merona de, B. and Boudou,
836 A., 2001. Goldmining activities and mercury contamination of native
837 Amerindian communities in french Guiana: key role of fish in dietary uptake.
838 Environ. Health Persp. 109: 449-456.
839 Fritsch, E., Bocquier, G., Boulet, R., Dosso, M. and Humbel, F.X., 1986.
840 Transforming systems of ferrallitic cover in French Guiana, structural analysis
841 of a supergene formation and mode of representation. ORSTOM notebook,
842 Pedol. Ser. 12(4): 361-395 (in French).
843 Fritsch, E., Morin, G., Bedidi, A., Bonnin, D., Balan, E., Caquineau, S. and Calas, G.,
844 2005. Transformation of haematite and Al-poor goethite to Al-rich goethite and
845 associated yellowing in a ferralitic clay soil profile of the middle Amazon Basin
846 (Manaus, Brazil). Eur. J. Soil Sci. 56(5): 575-588.
847 Fritsch, E., Herbillon, A.J., doNascimento, N.R., Grimaldi, M. and Melfi, A.J., 2006.
848 From Plinthic Acrisols to Plinthosols and Gleysols: iron and groundwater
849 dynamics in the tertiary sediments of the upper Amazon basin. Eur. J. Soil Sci.
850 58: 989-1006.
851 Gasper, J.D., Aiken, G.R. and Ryan, J.N., 2007. A critical review of three methods
852 used for the measurement of mercury (Hg^{2+})-dissolved organic matter stability
853 constants. Appl. Geochem. 22(8): 1583-1597.
854 Grimaldi, C., Grimaldi, M., Millet, A., Bariac, T. and Boulègue, J., 2004. Behavior of
855 chemical solutes during a storm in a rainforested headwater catchment.
856 Hydrol. Process. 18: 93-106.
857 Grimaldi, C., Guedron, S. and Grimaldi, M., 2008. Mercury distribution in tropical soil
858 profiles related to origin of mercury and soil processes. Sci. Total Environ.
859 401: 121-129.

860 Grimaldi, M., Gaudet, J.P., Grimaldi, C., Melieres, M.A. and Spadini, L., 2001.
861 Sources, budget and transfers in soils and sediments. In: CNRS (Editor),
862 Mercury in French Guiana research Program. Final report, part one: the region
863 of Saint Elie and the Petit Saut reservoir. CNRS-PEVS, pp. 5-15 (in French).
864 Guedron, S., Grimaldi, C., Chauvel, C., Spadini, C. and Grimaldi, M., 2006.
865 Weathering versus atmospheric contributions to mercury concentrations in
866 French Guiana soils. Appl. Geochem. 21: 2010-2022.
867 Guehl, J.M., 1984. Water dynamic in French Guiana tropical humid forest soil.
868 Influence of the pedological cover . Ann. For. Sci. 41(2): 195–236 (in French).
869 Kerndorff, H. and Schnitzer, M., 1980. Sorption of metals on humic acid . Geochim.
870 Cosmochim. Acta. 44: 1701-1708.
871 Khwaja, A., Bloom, P.R. and Brezonik, P.L., 2006. Binding constants of divalent
872 Mercury (Hg^{2+}) in soil humic acids and soil organic matter. Environ. Sci.
873 Technol. 40: 844-849.
874 Kim, C., Rytuba, J. and Brown, J.G.E., 2004a. EXAFS study of mercury (II) sorption
875 to Fe- and Al- (hydr)oxides I. Effect of chloride and sulfate. J. Colloid Interface
876 Sci. 270: 9-20.
877 Kim, C., Rytuba, J.J. and Brown, J.G.E., 2004b. EXAFS study of mercury (II) sorption
878 to Fe- and Al- (hydr)oxides I. Effect of pH. J. Colloid Interface Sci. 271: 1-15.
879 Kostka, J.E. and Luther III, G.W., 1994. Partitioning and speciation of solid phase
880 iron in saltmarsh sediments. Geochim. Cosmochim. Acta. 58(7): 1701–1710.
881 Lacerda, L.D., 1997. Global mercury emissions from gold and silver mining. Water
882 Air Soil Poll. 97: 209-221.
883 Lebel, J., Mergler, D., Lucotte, M., Amorin, M., Dolbec, J., Miranda, D., Arantes, G.,
884 Rhéault, I. and Pichet, P., 1996. Evidence of early nervous system disfunction

885 in Amazonian populations exposed to low levels of methylmercury.
886 Neurotoxicol. 17: 157-168.
887 Lechler, P.J., Miller, J.R., Hsu, L.-C. and Desilets, M.O., 1997. Mercury mobility at the
888 Carson River Superfund Site, west-central Nevada, USA: Interpretation of
889 mercury speciation data in mill tailings, soils, and sediments. J. Geochem.
890 Explor. 58(2-3): 259-267.
891 Lechler, P.J., Miller, J.R., Lacerda, L.D., Vinson, D., Bonzongo, J.-C., Lyons, W.B.
892 and Warwick, J.J., 2000. Elevated mercury concentrations in soils, sediments,
893 water, and fish of the Madeira River basin, Brazilian Amazon: a function of
894 natural enrichments? Sci. Total Environ. 260: 87-96.
895 Leermakers, M., Baeyens, W., Quevauviller, P. and Horvat, M., 2005. Mercury in
896 environmental samples: Speciation, artifacts and validation. Trends Anal.
897 Chem. 24(5): 383-393.
898 Lucas, Y., Nahon, D., Cornu, S. and Eyrolle, F., 1996. Soil genesis and dynamics in
899 equatorial areas. C. R. Acad. Sci. 322(1): 1-16 (In French).
900 Malengreau, N. and Sposito, G., 1997. Short-time dissolution mechanisms of
901 kaolinitic tropical soils. Geochim. Cosmochim. Acta; 61(20): 4297-4307.
902 Manceau, A. and Nagy, K.L., 2008. Relationships between Hg(II)–S bond distance
903 and Hg(II) coordination in thiolates. Dalton Trans. 11: 1385–1508.
904 Mikac, N., Foucher, D., Niessen, S. and Fischer, J.-C., 2002. Extractability of HgS
905 (cinnabar and metacinnabar) by hydrochloric acid. Anal. Bioanal. Chem.
906 374(6): 1028-1033.
907 Mikac, N., Foucher, D., Niessen, S., Lojen, S. and Fischer, J.-C., 2003. Influence of
908 chloride and sediment matrix on the extractability of HgS (cinnabar and
909 metacinnabar) by nitric acid. Anal. Bioanal. Chem. 377(7): 1196-1201.

910 Milési, J.P., Egal, E., Ledru, P., Vernhet, Y., Thiéblemont, D., Cocherie, A., Tegyey,
911 M., Martel-Jantin, B. and Lagny, P., 1995. Mineralizations of the northern
912 French Guiana in their geological setting. Mining Res. Chron. 518: 5-58 (in
913 French).
914 Molicova, H., Grimaldi, M., Bonell, M. and Hubert, P., 1997. Using TOPMODEL
915 towards identifying and modelling the hydrological patterns within a headwater
916 humid, tropical catchment. Hydrolog. Process. 11: 1169-1196.
917 Ochs, M., Cosovic, B. and Stumm, W., 1994. Coordinative and hydrophobic
918 interaction of humic substances with hydrophilic Al_2O_3 and hydrophobic
919 mercury surfaces. Geochim. Cosmochim. Acta. 58(2): 639-650.
920 Richard, S., Arnoux, A., Cerdan, P., Reynouard, C. and Horeau, V., 2000. Mercury
921 levels of soils, sediments and fish in French Guiana, South America. Water Air
922 Soil Poll. 124: 221-244.
923 Rodriguez Martin-Doimeadios, R.C., Wasserman, J.C., Garcia Bermejo, L.F.,
924 Amouroux, D., Berzas Nevado, J.J. and Donard, O.F.X., 2000. Chemical
925 availability of mercury in stream sediments from the Almaden area, Spain. J.
926 Environ. Monit. 2: 360-366.
927 Roos-Barraclough, F., Givelet, N., Martinez-Cortizas, A., Goodsite, M.E., Biester, H.
928 and Shotyk, W., 2002. An analytical protocol for determination of total mercury
929 concentration in solid peat samples. Sci. Tot. Environ. 292: 129-139.
930 Roulet, M. and Lucotte, M., 1995. Geochemistry of mercury in pristine and flooded
931 ferralitic soil of a tropical rain forest in French Guiana, South America. Water,
932 Air, Soil Poll. 80: 1079-1088.
933 Roulet, M., Lucotte, M., Saint-Aubin, A., Tran, S., Rheault, I., Farella, N., Da Silva,
934 E.D., Dezencourt, J., Passos, C.J.S., Soares, G.S., Guimaraes, J.R.D.,

935 Mergler, D. and Amorim, M., 1998. The geochemistry of mercury in central
936 Amazonian soils developed on the Alter-do-Chao formation of the lower
937 Tapajos River Valley, Para state, Brazil. Sci. Total Environ. 223(1): 1-24.
938 Rowell, D.L., 1994. Soil Science : methods and applications. British Library, Harlow
939 (England).
940 Sanchez, D.M., Quejido, A.J., Fernandez, M., Hernandez, C., Schmid, T., Millan, R.,
941 Gonzalez, M., Aldea, M., Martan, R. and Morante, R., 2005. Mercury and trace
942 element fractionation in Almaden soils by application of different sequential
943 extraction procedures. Anal. Bioanal. Chem. 381(8): 1507-1513.
944 Sarkar, D., Essington, M.E. and Misra, K.C., 1999. Adsorption of mercury(II) by
945 variable charge surfaces of quartz and gibbsite. Soil Sci. Soc. Am. J. 63:
946 1626-1636.
947 Sarkar, D., Essington, M.E. and Misra, K.C., 2000. Adsorption of mercury(II) by
948 kaolinite. Soil Sci. Soc. Am. J. 64: 1698-1975.
949 Schnitzer, M. and Kerndorff, H., 1981. Reactions of fulvic acid with metal ions. Water,
950 Air, Soil Poll. 15: 97-108.
951 Schulze, D.G., 1984. The influence of aluminium on iron oxides. VIII. Unit-cell
952 dimension of Al-substituted goethites and estimation of Al from them. Clays
953 Clay Miner. 32(1): 36-44.
954 Schuster, E., 1991. The behavior of mercury in the soil with special emphasis on
955 complexation and adsorption processes- a review of the literature. Water Air
956 Soil Poll. 56: 667-680.
957 Schwertmann, U. and Latham, M., 1986. Properties of iron oxides in some new
958 caledonian oxisols. Geoderma. 39: 105-123.

959 Schwertmann, U. and Cornell, R.M., 2000. Iron oxides in the laboratory : preparation
960 and characterization. Wiley-VCH, Weinheim, 188 pp.
961 Shannon, R., 1976. Revised effective ionic radii and systematic studies of interatomic
962 distances in halides and chalcogenides. Acta Crystallogr. 32(5): 751-767.
963 Skyllberg, U., Xia, K., Bloom, P.R., Nater, E.A. and Bleam, W.F., 2000. Binding of
964 mercury(II) to reduced sulfur in soil organic matter along upland-peat soil
965 transects. J. Environ. Qual. 29: 855-865.
966 Skyllberg, U., Bloom, P.R., Qian, J., Lin, C.-M. and Bleam, W.F., 2006. Complexation
967 of Mercury(II) in Soil Organic Matter: EXAFS Evidence for Linear Two-
968 Coordination with Reduced Sulfur Groups. Environ. Sci. Technol. 40(13):
969 4174-4180.
970 Sladek, C. and Gustin, M.S., 2003. Evaluation of sequential and selective extraction
971 methods for determination of mercury speciation and mobility in mine waste.
972 Appl. Geochem. 18(4): 567-576.
973 Slowey, A.J., Rytuba, J.J. and Brown, J.G.E., 2005. Speciation of mercury and mode
974 of transport from placer Gold Mine Tailings. Environ. Sci. Technol. 39(6):
975 1547-1554.
976 Slowey, A.J. and Brown, J.G.E., 2007. Transformations of mercury, iron, and sulfur
977 during the reductive dissolution of iron oxyhydroxide by sulfide. Geochim.
978 Cosmochim. Acta. 71(4): 877-894.
979 Stanjek, H. and Schwertmann, U., 1992. The influence of aluminium on iron oxides.
980 Part XVI: hydroxyl and aluminium substitution on synthetic hematites. Clays
981 Clay Miner. 40(3): 347-354.
982 Tandy, J.C., Grimaldi, M., Grimaldi, C. and Tessier, D., 1990. Mineralogical and
983 textural changes in French Guiana oxisols and their relation with

984 microaggregation. In: L.A. Douglas (Editor), Soil micromorphology. A basic
985 and applied science. 8. International Working Meeting of Soil
986 Micromorphology. Developments in Soil Science. Elsevier, Amsterdam, pp.
987 191-198.
988 Trivedi, P. and Axe, L., 2001. Ni and Zn Sorption to Amorphous versus Crystalline
989 Iron Oxides: Macroscopic Studies. J. Colloid Interface Sci., 244: 221-229.
990 Veiga, M. and Baker, R., 2004. Protocols for environmental and health assessment
991 of mercury released by artisanal and small scale miners. Report to the Global
992 mercury project: removal of barriers to introduction of cleaner artisanal gold
993 mining and extraction technologies, GEF/UNDP/UNIDO; 2004. p. 170.
994 Velasquez, E., Pelosi, C., Brunet, D., Grimaldi, M., Martins, M., Rendeiro, A.C.,
995 Barrios, E. and Lavelle, P., 2007. This ped is my ped: Visual separation and
996 near infrared spectra allow determination of the origins of soil
997 macroaggregates. Pedobiologia. 51(1): 75-87.
998 Wallschlager, D., Desai, M.V.M., Spengler, M. and Wilken, R.-D., 1998. Mercury
999 speciation in floodplain soils and sediments along a contaminated river
1000 transect. J. Environ. Qual. 27: 1034-1044.
1001 Webster, R., 2001. Statistics to support soil research and their presentation. Eur. J.
1002 Soil Sci. 52(2): 331-340.
1003 Weerasooriya, R., Tobschall, H.J., Seneviratne, W. and Bandara, A., 2007.
1004 Transition state kinetics of Hg(II) adsorption at gibbsite-water interface. J.
1005 Hazard. Mater. 147(3): 971-978.
1006 Wentworth, C.K., 1922. A scale of grade and class terms for clastic sediments. J.
1007 Geol. 30: 377-392.
1008

Table 1: Pearson correlation matrix (correlation coefficient (CC), P value (P) and number of samples (N)) of pristine soils extracted Hg, Hg extraction yields, Fe, Al, Clay size fraction, Fine silts, C and S for total and (a) HCl/HNO_3 (labeled HCl) and ascorbate (labeled Asco) selective extractions, and (b) KOH and NH_4OH selective extractions.

Table 1a

	Statistics	$[Hg]_{HCl}$ (µg g^{-1})	$(Hg)_{HCl}$ (%)	$[Fe]_{HCl}$ (mg g^{-1})	$[Al]_{HCl}$ (mg g^{-1})	Clay (g/100g)	Silt (g/100g)	C (g/100g)	S (g/100g)
[HgT] (µg g^{-1})	CC	**1.00**	0.45	0.19	0.15	**0.59**	- 0.60	**0.42**	**0.62**
	P	1.E-41	3.E-03	2.E-01	3.E-01	9.E-05	7.E-05	7.E-03	2.E-05
	N	40	40	40	40	38	38	40	40
$[Hg]_{HCl}$ (µg g^{-1})	CC		0.48	0.18	0.13	**0.56**	- 0.57	0.40	**0.58**
	P		2.E-03	3.E-01	4.E-01	3.E-04	2.E-04	1.E-02	9.E-05
	N		40	40	40	38	38	40	40
$(Hg)_{HCl}$ (%)	CC			0.25	0.16	0.38	- 0.44	0.31	0.28
	P			1.E-01	3.E-01	2.E-02	6.E-03	5.E-02	8.E-02
	N			40	40	38	38	40	40
$[Fe]_{HCl}$ (mg g^{-1})	CC				**0.69**	0.34	- 0.33	0.16	0.24
	P				8.E-07	4.E-02	4.E-02	3.E-01	1.E-01
	N				40	38	38	40	40
$[Al]_{HCl}$ (mg g^{-1})	CC					**0.57**	- 0.42	0.12	0.39
	P					2.E-04	9.E-03	5.E-01	1.E-02
	N					38	38	40	40
Clay (g/100g)	CC						- 0.80	0.37	**0.80**
	P						3.E-09	2.E-02	2.E-09
	N						38	38	38
Silt (g/100g)	CC							- 0.57	- 0.70
	P							2.E-04	1.E-06
	N							38	38
C (g/100g)	CC								**0.47**
	P								0.00251
	N								40

	$[Hg]_{KOH}$ (µg g^{-1})	$(Hg)_{KOH}$ (%)	$[Fe]_{KOH}$ (mg g^{-1})	$[Al]_{KOH}$ (mg g^{-1})	Clay (g/100g)	Silt (g/100g)	C (g/100g)	S (g/100g)
[HgT] (µg g^{-1})	**0.89**	0.32	0.33	0.37	**0.59**	- 0.60	**0.42**	**0.62**
	7.E-14	5.E-02	5.E-02	3.E-02	9.E-05	7.E-05	7.E-03	2.E-05
	38	38	36	36	38	38	40	40
$[Hg]_{KOH}$ (µg g^{-1})		0.63	0.21	0.15	0.48	- 0.42	0.26	**0.51**
		2.E-05	2.E-01	4.E-01	3.E-03	1.E-02	1.E-01	1.E-03
		38	36	36	36	36	38	38
$(Hg)_{KOH}$ (%)			- 0.02	- 0.10	0.38	- 0.28	0.15	0.33
			9.E-01	6.E-01	2.E-02	1.E-01	4.E-01	4.E-02
			36	36	36	36	38	38
$[Fe]_{KOH}$ (mg g^{-1})				**0.60**	**0.62**	- 0.38	- 0.15	**0.48**
				1.E-04	1.E-04	2.E-02	4.E-01	3.E-03
				36	34	34	36	36
$[Al]_{KOH}$ (mg g^{-1})					**0.68**	- 0.48	0.16	**0.50**
					1.E-05	4.E-03	4.E-01	2.E-03
					34	34	36	36
Clay (g/100g)						- 0.80	0.37	**0.80**
						3.E-09	2.E-02	2.E-09
						38	38	38
Silt (g/100g)							- 0.57	- 0.70
							2.E-04	1.E-06
							38	38
C (g/100g)								**0.47**
								3.E-03
								40

Table 1b

	Statistics	$[Hg]_{Asco}$ (µg g^{-1})	$(Hg)_{Asco}$ (%)	$[Fe]_{Asco}$ (mg g^{-1})	$[Al]_{Asco}$ (mg g^{-1})	Clay (g/100g)	Silt (g/100g)	C (g/100g)	S (g/100g)
[HgT] (µg g^{-1})	CC	**0.77**	0.21	0.40	0.35	**0.59**	- 0.60	**0.42**	**0.62**
	P	1.E-08	2.E-01	1.E-02	3.E-02	9.E-05	7.E-05	7.E-03	2.E-05
	N	39	39	40	40	38	38	40	40
$[Hg]_{Asco}$ (µg g^{-1})	CC		0.73	**0.68**	**0.60**	**0.64**	- 0.66	**0.56**	**0.59**
	P		2.E-07	2.E-06	5.E-05	2.E-05	9.E-06	2.E-04	8.E-05
	N		39	39	39	37	37	39	39
$(Hg)_{Asco}$ (%)	CC			0.62	0.51	0.39	- 0.35	0.37	0.32
	P			3.E-05	9.E-04	2.E-02	4.E-02	2.E-02	4.E-02
	N			39	39	37	37	39	39
$[Fe]_{Asco}$ (mg g^{-1})	CC				**0.98**	0.42	- 0.52	0.30	0.37
	P				3.E-27	8.E-03	7.E-04	6.E-02	2.E-02
	N				40	38	38	40	40
$[Al]_{Asco}$ (mg g^{-1})	CC					0.37	- 0.47	0.22	0.31
	P					2.E-02	3.E-03	2.E-01	5.E-02
	N					38	38	40	40
Clay (g/100g)	CC						- 0.80	**0.37**	**0.80**
	P						3.E-09	2.E-02	2.E-09
	N						38	38	38
Silt (g/100g)	CC							- 0.57	- 0.70
	P							2.E-04	1.E-06
	N							38	38
C (g/100g)	CC								**0.47**
	P								3.E-03
	N								40

	$[Hg]_{NH4OH}$ (µg g^{-1})	$(Hg)_{NH4OH}$ (%)	$[Fe]_{NH4OH}$ (mg g^{-1})	$[Al]_{NH4OH}$ (mg g^{-1})	Clay (g/100g)	Silt (g/100g)	C (g/100g)	S (g/100g)
[HgT] (µg g^{-1})	**0.90**	**0.45**	0.27	0.08	**0.59**	- 0.60	**0.42**	**0.62**
	2.E-15	4.E-03	1.E-01	6.E-01	9.E-05	7.E-05	7.E-03	2.E-05
	40	40	39	40	38	38	40	40
$[Hg]_{NH4OH}$ (µg g^{-1})		0.74	0.31	0.08	**0.70**	- 0.70	**0.65**	**0.71**
		4.E-08	6.E-02	6.E-01	1.E-06	9.E-07	7.E-06	3.E-07
		40	39	40	38	38	40	40
$(Hg)_{NH4OH}$ (%)			0.23	0.06	0.68	- 0.68	0.67	0.67
			2.E-01	7.E-01	3.E-06	3.E-06	2.E-06	2.E-06
			39	40	38	38	40	40
$[Fe]_{NH4OH}$ (mg g^{-1})				**0.64**	0.06	- 0.24	0.23	0.15
				1.E-05	7.E-01	2.E-01	2.E-01	4.E-01
				39	37	37	39	39
$[Al]_{NH4OH}$ (mg g^{-1})					- 0.01	- 0.22	0.06	- 0.07
					9.E-01	2.E-01	7.E-01	7.E-01
					38	38	40	40
Clay (g/100g)						- 0.80	**0.37**	**0.80**
						3.E-09	2.E-02	2.E-09
						38	38	38
Silt (g/100g)							- 0.57	- 0.70
							2.E-04	1.E-06
							38	38
C (g/100g)								**0.47**
								3.E-03
								40

Table 2: Pearson correlation matrix (correlation coefficient (CC), P value (P) and number of samples (N)) of contaminated soils extracted Hg, Hg extraction yields, Fe, Al, Clay size fraction, Fine silts, C and S for total and (a) HCl/HNO_3 (labeled HCl) and ascorbate (labeled Asco) selective extractions, and (b) KOH and NH_4OH selective extractions.

Table 2a

	Statistics	$[Hg]_{HCl}$ (µg g^{-1})	$(Hg)_{HCl}$ (%)	$[Fe]_{HCl}$ (mg g^{-1})	$[Al]_{HCl}$ (mg g^{-1})	Clay (g/100g)	Sand (g/100g)	C (g/100g)	S (g/100g)
[HgT] (µg g^{-1})	CC	**1.00**	0.22	- 0.29	- 0.34	- 0.52	**0.50**	- 0.09	- 0.08
	P	4.E-86	2.E-01	8.E-02	4.E-02	1.E-03	2.E-03	6.E-01	7.E-01
	N	37	37	37	37	37	37	37	37
$[Hg]_{HCl}$ (µg g^{-1})	CC		0.22	- 0.30	- 0.35	- 0.52	**0.50**	- 0.09	- 0.08
	P		2.E-01	8.E-02	4.E-02	1.E-03	2.E-03	6.E-01	7.E-01
	N		37	37	37	37	37	37	37
$(Hg)_{HCl}$ (%)	CC			- 0.50	- 0.80	- 0.14	**0.22**	0.21	0.19
	P			2.E-03	3.E-09	4.E-01	2.E-01	2.E-01	3.E-01
	N			37	37	37	37	37	37
$[Fe]_{HCl}$ (mg g^{-1})	CC				**0.86**	0.37	- 0.32	- 0.14	- 0.08
	P				8.E-12	3.E-02	5.E-02	4.E-01	6.E-01
	N				37	37	37	37	37
$[Al]_{HCl}$ (mg g^{-1})	CC					0.42	- 0.41	- 0.11	- 0.07
	P					1.E-02	1.E-02	5.E-01	7.E-01
	N					37	37	37	37
Clay (g/100g)	CC						- 0.85	0.05	0.09
	P						4.E-11	8.E-01	6.E-01
	N						37	37	37
Sand (g/100g)	CC							- 0.38	- 0.41
	P							2.E-02	1.E-02
	N							37	37
C (g/100g)	CC								**0.94**
	P								2.1E-18
	N								37

	$[Hg]_{KOH}$ (µg g^{-1})	$(Hg)_{KOH}$ (%)	$[Fe]_{KOH}$ (mg g^{-1})	$[Al]_{KOH}$ (mg g^{-1})	Clay (g/100g)	Sand (g/100g)	C (g/100g)	S (g/100g)
[HgT] (µg g^{-1})	**0.88**	0.22	- 0.21	- 0.38	- 0.52	**0.50**	- 0.09	- 0.08
	2.E-12	2.E-01	2.E-01	2.E-02	1.E-03	2.E-03	6.E-01	7.E-01
	35	35	37	37	37	37	37	37
$[Hg]_{KOH}$ (µg g^{-1})		0.55	- 0.20	- 0.29	- 0.46	**0.52**	- 0.27	- 0.25
		7.E-04	3.E-01	9.E-02	6.E-03	1.E-03	1.E-01	1.E-01
		35	35	35	35	35	35	35
$(Hg)_{KOH}$ (%)			0.01	0.18	- 0.04	**0.26**	- 0.40	- 0.34
			9.E-01	3.E-01	8.E-01	1.E-01	2.E-02	4.E-02
			35	35	35	35	35	35
$[Fe]_{KOH}$ (mg g^{-1})				**0.54**	0.37	- 0.29	0.00	0.04
				6.E-04	3.E-02	8.E-02	1.E+00	8.E-01
				37	37	37	37	37
$[Al]_{KOH}$ (mg g^{-1})					**0.57**	- 0.49	0.09	0.22
					2.E-04	2.E-03	6.E-01	2.E-01
					37	37	37	37
Clay (g/100g)						- 0.85	0.05	0.09
						4.E-11	8.E-01	6.E-01
						37	37	37
Sand (g/100g)							- 0.38	- 0.41
							2.E-02	1.E-02
							37	37
C (g/100g)								**0.94**
								2.E-18
								37

Table 2b

	Statistics	$[Hg]_{Asco}$ (µg g^{-1})	$(Hg)_{Asco}$ (%)	$[Fe]_{Asco}$ (mg g^{-1})	$[Al]_{Asco}$ (mg g^{-1})	Clay (g/100g)	Sand (g/100g)	C (g/100g)	S (g/100g)
[HgT] (µg g^{-1})	CC	**0.89**	- 0.23	- 0.27	- 0.40	- 0.52	**0.50**	- 0.09	- 0.08
	P	1.E-13	2.E-01	1.E-01	2.E-02	1.E-03	2.E-03	6.E-01	7.E-01
	N	37	37	36	36	37	37	37	37
$[Hg]_{Asco}$ (µg g^{-1})	CC		0.12	- 0.34	- 0.45	- 0.53	**0.48**	0.04	0.02
	P		5.E-01	4.E-02	6.E-03	8.E-04	3.E-03	8.E-01	9.E-01
	N		37	36	36	37	37	37	37
$(Hg)_{Asco}$ (%)	CC			- 0.26	- 0.00	0.25	- 0.25	0.39	0.35
	P			1.E-01	1.E+00	1.E-01	1.E-01	2.E-02	3.E-02
	N			36	36	37	37	37	37
$[Fe]_{Asco}$ (mg g^{-1})	CC				**0.85**	0.30	- 0.32	- 0.10	- 0.03
	P				8.E-11	8.E-02	6.E-02	6.E-01	9.E-01
	N				36	36	36	36	36
$[Al]_{Asco}$ (mg g^{-1})	CC					**0.56**	- 0.53	0.06	0.17
	P					4.E-04	8.E-04	7.E-01	3.E-01
	N					36	36	36	36
Clay (g/100g)	CC						- 0.85	0.05	0.09
	P						4.E-11	8.E-01	6.E-01
	N						37	37	37
Sand (g/100g)	CC							- 0.38	- 0.41
	P							2.E-02	1.E-02
	N							37	37
C (g/100g)	CC								**0.94**
	P								2.E-18
	N								37

	$[Hg]_{NH4OH}$ (µg g^{-1})	$(Hg)_{NH4OH}$ (%)	$[Fe]_{NH4OH}$ (mg g^{-1})	$[Al]_{NH4OH}$ (mg g^{-1})	Clay (g/100g)	Sand (g/100g)	C (g/100g)	S (g/100g)
[HgT] (µg g^{-1})	**0.96**	0.10	- 0.15	- 0.27	- 0.52	**0.50**	- 0.09	- 0.08
	7.E-21	5.E-01	4.E-01	1.E-01	1.E-03	2.E-03	6.E-01	7.E-01
	37	37	37	37	37	37	37	37
$[Hg]_{NH4OH}$ (µg g^{-1})		0.31	- 0.18	- 0.25	- 0.50	**0.53**	- 0.15	- 0.13
		6.E-02	3.E-01	1.E-01	1.E-03	8.E-04	4.E-01	4.E-01
		37	37	37	37	37	37	37
$(Hg)_{NH4OH}$ (%)			- 0.08	0.14	- 0.02	0.18	- 0.13	- 0.05
			7.E-01	4.E-01	9.E-01	3.E-01	5.E-01	8.E-01
			37	37	37	37	37	37
$[Fe]_{NH4OH}$ (mg g^{-1})				0.41	0.37	- 0.32	**0.47**	**0.43**
				1.E-02	2.E-02	5.E-02	3.E-03	7.E-03
				37	37	37	37	37
$[Al]_{NH4OH}$ (mg g^{-1})					0.46	- 0.44	0.23	0.33
					4.E-03	7.E-03	2.E-01	5.E-02
					37	37	37	37
Clay (g/100g)						- 0.85	0.05	0.09
						4.E-11	8.E-01	6.E-01
						37	37	37
Sand (g/100g)							- 0.38	- 0.41
							2.E-02	1.E-02
							37	37
C (g/100g)								**0.94**
								2.E-18
								37

Figure captions

Fig. 1: Top left: french Guiana map with the studied site location (closed circle). Right and bottom: detailed map of the studied site, including general watershed scheme with soil sampling locations, and associated legend.

Fig. 2: Evolutions with depth of total Hg, C and C/N ratio for (a) pristine and (b) contaminated soils. Evolutions with depth of the clay- and sand-size fractions are reported for pristine and contaminated soils, respectively.

Fig. 3: XRD patterns normalized on quartz peak (refer to the text for details) for raw samples, and following ascorbate, KOH, NH_4OH and HCl/HNO_3 extractions.

Fig. 4: Top : Evolutions with depth of Fe and Al concentrations extracted by ascorbate and corresponding Al/Fe ratio. Bottom: same graphs as top, focused on calculated crystalline + residual fraction in pristine soils.

Fig. 5: Evolutions with depth of $(Hg)_{HCl/HNO3}$, $(Hg)_{CR}$, $(Hg)_{Asco}$, $(Hg)_{NH4OH}$, and $(Hg)_{KOH}$ extraction yield (%) in pristine soils. Triangles, circles and squares refer to toposequence I, II and III, and white, grey and black filled colours refer to ferralsols, acrisols and gleysols, respectively.

Fig. 6: XRD patterns of nodules from pristine soils I-2 (10-20cm), I-2 (30-40cm), and I-2 (180-200cm).

Fig. 7: µXRF mapping of Si, K, Fe, Au and Hg of SL6 (30-50 cm) sample and counts measured on Lα edge fluorescence of Hg and Au versus Kα radiation of Si, K and Fe, and comparison on counts measured for Hg (Y axis) versus Au (X axis).

Fig. 8: Evolution with depth of $(Hg)_{HCl/HNO3}$, $(Hg)_{CR}$, $(Hg)_{Asco}$, $(Hg)_{NH4OH}$, $(Hg)_{KOH}$ and (Hg^0) pyrolysis extraction yields (%) in contaminated soils.

Fig. 1.

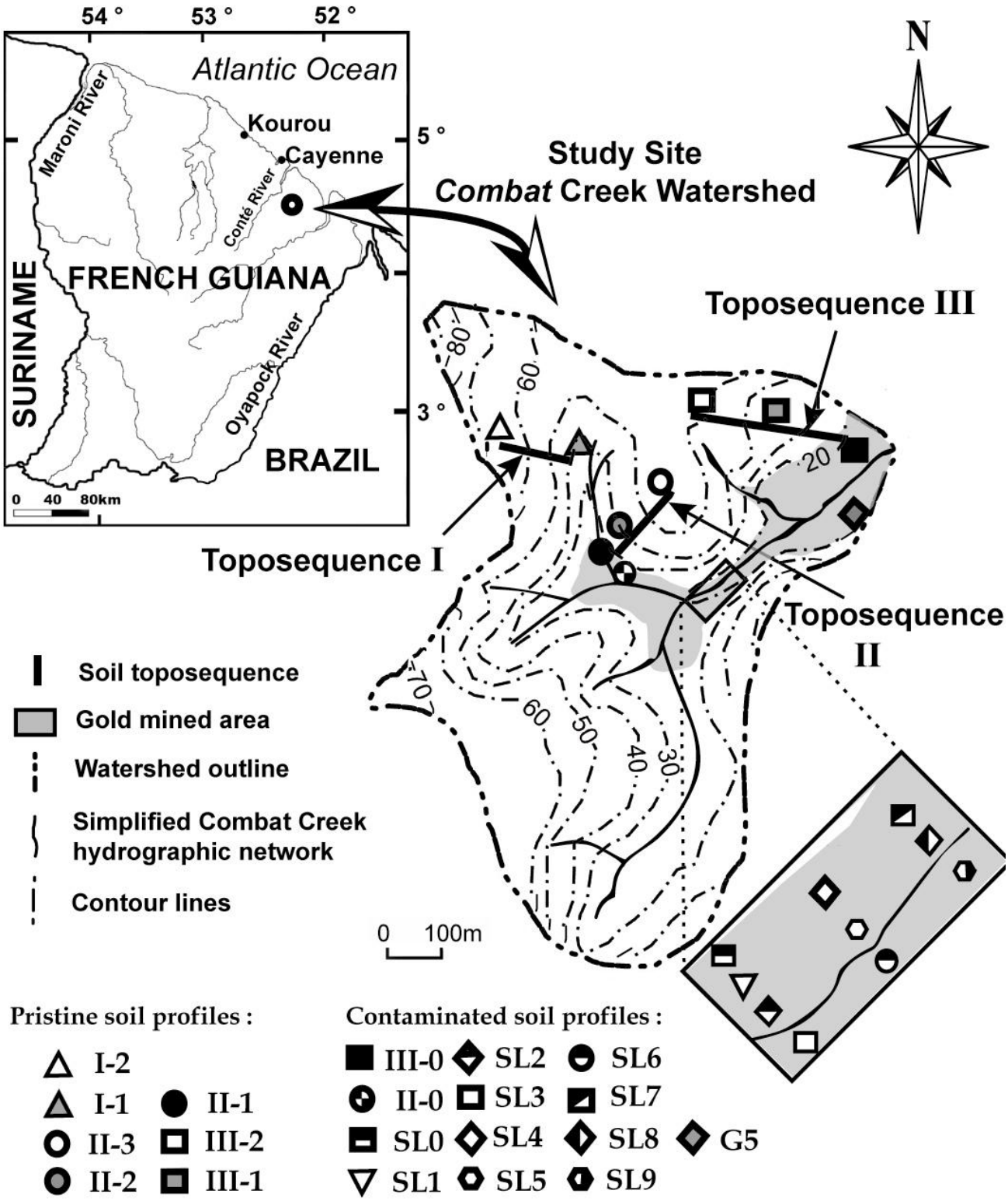
54 °
53 °
52 °
Atlantic Ocean
Maroni River
Kourou
Cayenne
5 °
Conté River
FRENCH GUIANA
SURINAME
Oyapock River
3 °
BRAZIL
0 40 80km
N
Study Site
Combat Creek Watershed
Toposequence III
Toposequence I
Toposequence II
80
60
20
70
60
50
40
30
Soil toposequence
Gold mined area
Watershed outline
Simplified Combat Creek hydrographic network
Contour lines
0 100m
Pristine soil profiles :
I-2
I-1
II-1
II-3
III-2
II-2
III-1
Contaminated soil profiles :
III-0
SL2
SL6
II-0
SL3
SL7
SL0
SL4
SL8
G5
SL1
SL5
SL9

Fig. 2.a.

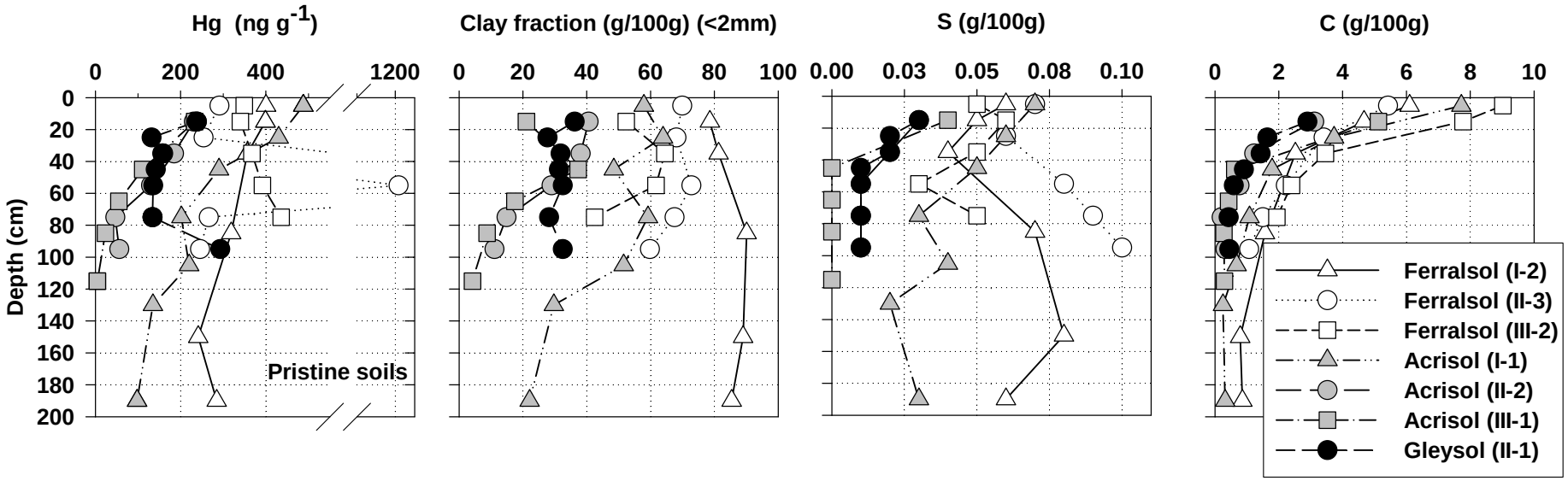
Hg (ng g-1)
Clay fraction (g/100g) (<2mm)
S (g/100g)
C (g/100g)
Depth (cm)
Pristine soils
Ferralsol (I-2)
Ferralsol (II-3)
Ferralsol (III-2)
Acrisol (I-1)
Acrisol (II-2)
Acrisol (III-1)
Gleysol (II-1)

Fig. 2.b.

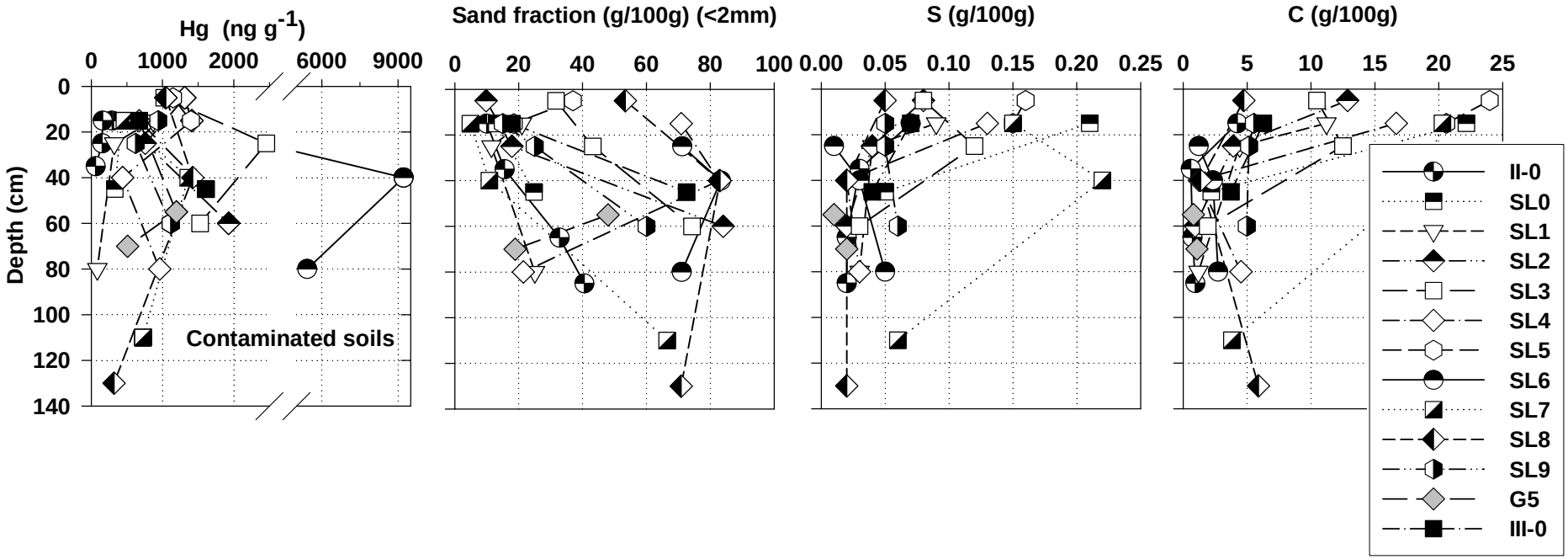
Hg (ng g-1)
Sand fraction (g/100g) (<2mm)
S (g/100g)
C (g/100g)
Depth (cm)
Contaminated soils
II-0
SL0
SL1
SL2
SL3
SL4
SL5
SL6
SL7
SL8
SL9
G5
III-0

Fig. 3.

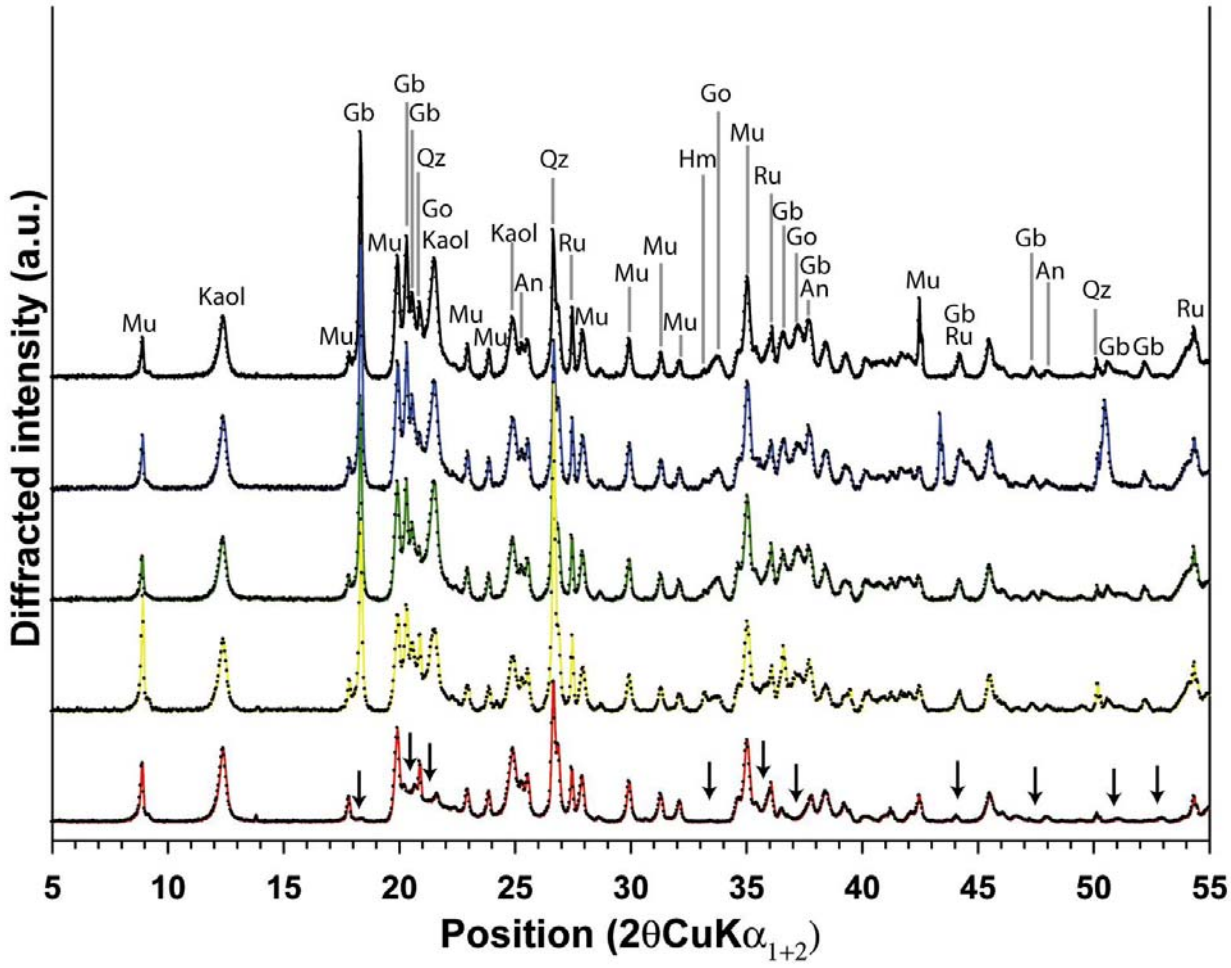
Diffracted intensity (a.u.)
Position (2θCuKα1+2)
5
10
15
20
25
30
35
40
45
50
55
Mu
Kaol
Gb
Qz
Go
An
Hm
Ru
Mu
Gb
Gb
Qz
Go
Kaol
Mu
Kaol
An
Qz
Ru
Mu
Mu
Mu
Go
Mu
Ru
Gb
Go
Gb
An
Mu
Gb
Ru
Gb
An
Qz
Gb
Gb
Ru

Fig. 4.

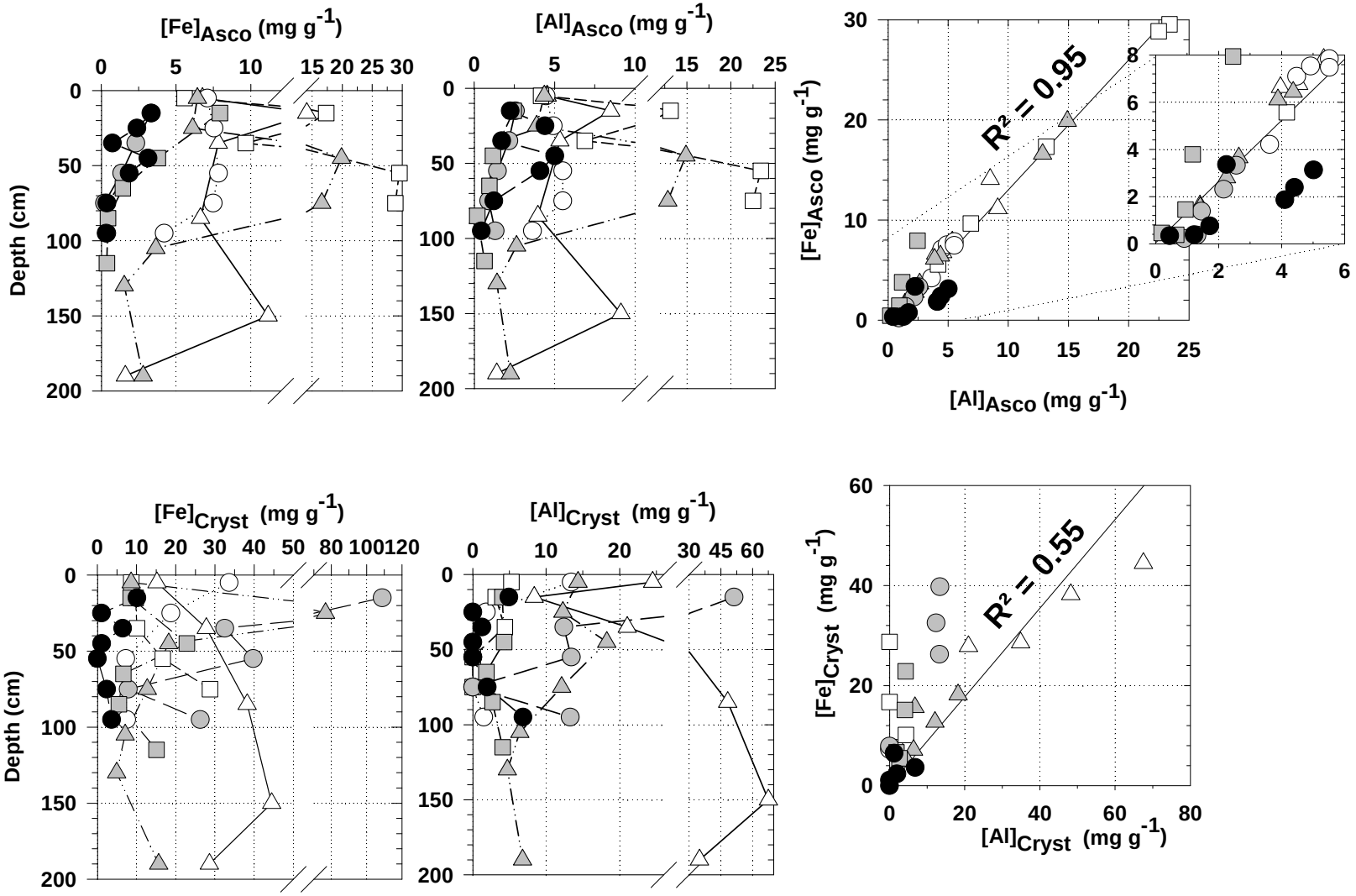
[Fe]Asco (mg g-1)
[Al]Asco (mg g-1)
Depth (cm)
R² = 0.95
[Fe]Asco (mg g-1)
[Al]Asco (mg g-1)
[Fe]Cryst (mg g-1)
[Al]Cryst (mg g-1)
Depth (cm)
R² = 0.55
[Fe]Cryst (mg g-1)
[Al]Cryst (mg g-1)

Fig. 5.

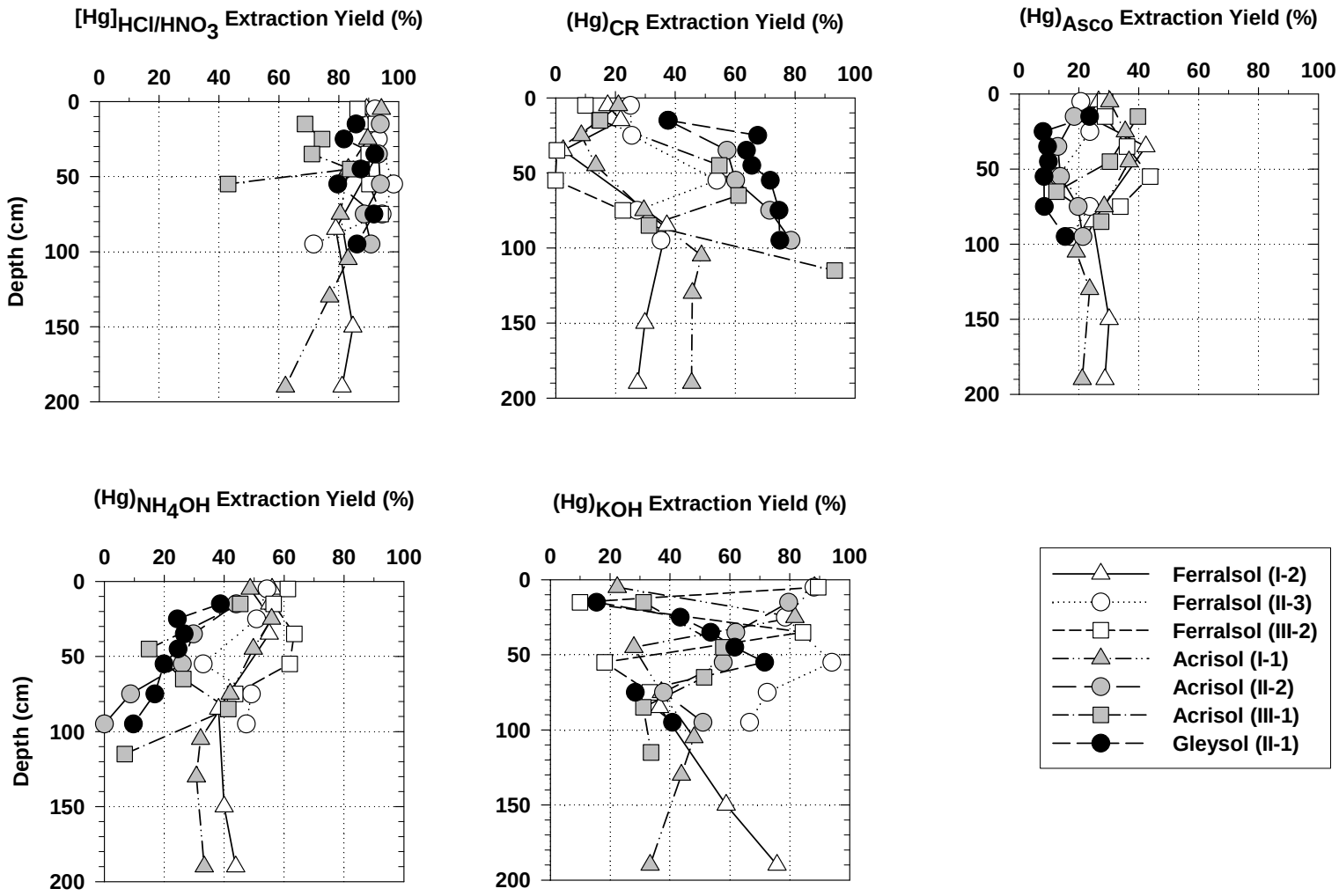
[Hg]HCl/HNO3 Extraction Yield (%)
(Hg)CR Extraction Yield (%)
(Hg)Asco Extraction Yield (%)
(Hg)NH4OH Extraction Yield (%)
(Hg)KOH Extraction Yield (%)
Depth (cm)
0
20
40
60
80
100
50
150
200
Ferralsol (I-2)
Ferralsol (II-3)
Ferralsol (III-2)
Acrisol (I-1)
Acrisol (II-2)
Acrisol (III-1)
Gleysol (II-1)

Fig. 6.

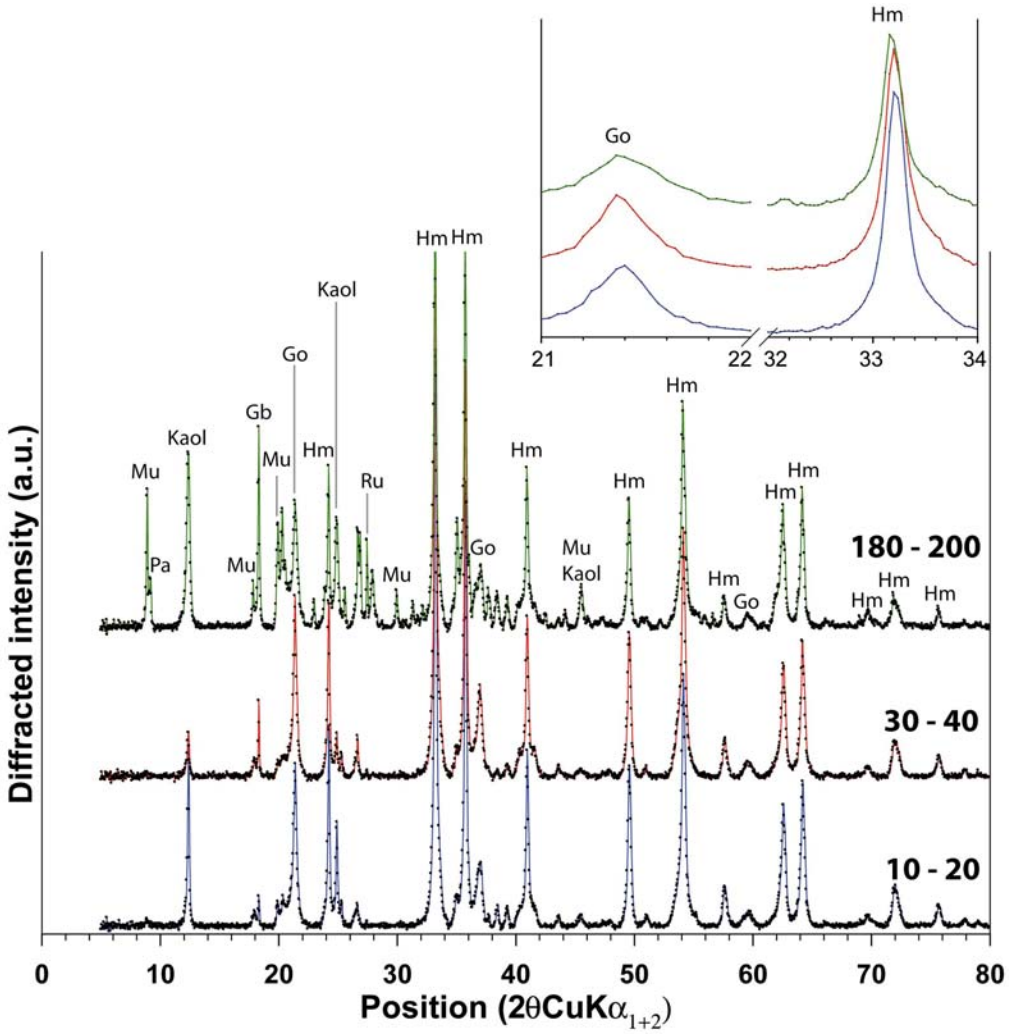
Diffracted intensity (a.u.)
Position (2θCuKα1+2)
180 - 200
30 - 40
10 - 20
Mu
Pa
Kaol
Gb
Mu
Go
Mu
Hm
Kaol
Ru
Mu
Hm Hm
Go
Hm
Mu
Kaol
Hm
Hm
Go
Hm
Hm
Hm
Hm
Hm
Hm
Go
21
22
32
33
34
0
10
20
30
40
50
60
70
80

Fig . 7.

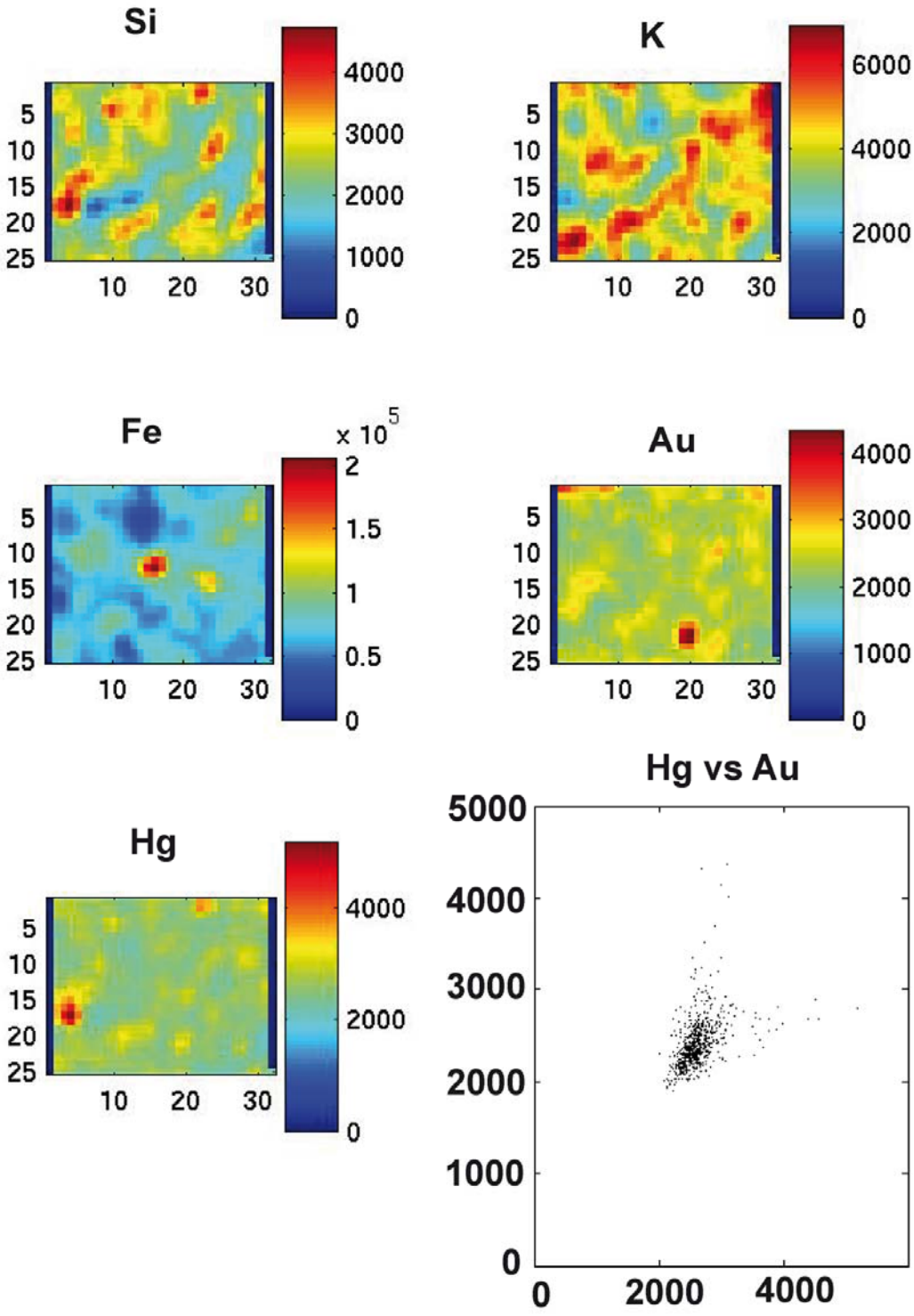
Si
4000
3000
2000
1000
0
K
6000
4000
2000
0
Fe
x 10^5
2
1.5
1
0.5
0
Au
4000
3000
2000
1000
0
Hg
4000
2000
0
Hg vs Au
5000
4000
3000
2000
1000
0
0
2000
4000
5
10
15
20
25
10
20
30

Fig . 8.

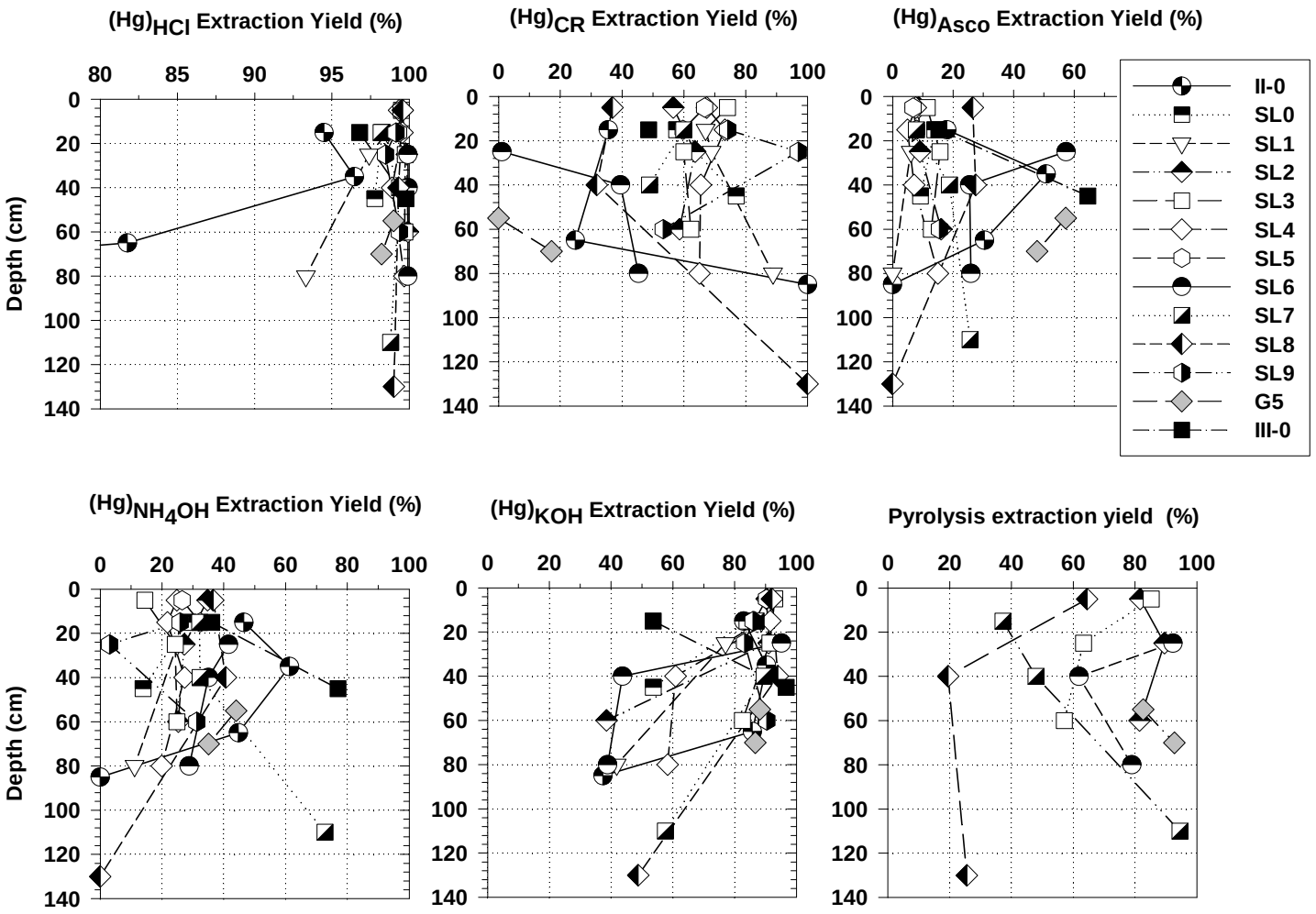
(Hg)HCl Extraction Yield (%)
(Hg)CR Extraction Yield (%)
(Hg)Asco Extraction Yield (%)
(Hg)NH4OH Extraction Yield (%)
(Hg)KOH Extraction Yield (%)
Pyrolysis extraction yield (%)
Depth (cm)
II-0
SL0
SL1
SL2
SL3
SL4
SL5
SL6
SL7
SL8
SL9
G5
III-0

Supplementary data 2

(Electronic table)

Table E1: Percent recoveries of Hg in supernatant and solid residue for Certified materials CRM 7002, MESS-3 and sample I-1 (0-10 cm) for ascorbate, NH_4OH , KOH and HCl/HNO_3 selective extractions.

	Ascorbate			NH_4OH		KOH			HCl/HNO_3		
Sample	**CRM 7002**	**MESS- 3**	**I-1 (0-10 cm)**	**CRM 7002**	**MESS- 3**	**CRM 7002**	**MESS- 3**	**I-1 (0-10 cm)**	**CRM 7002**	**MESS- 3**	**I-1 (0-10 cm)**
Mean	98.8	68.7	60.4	102.1	93.5	106.5	96.4	87.9	101.0	114.9	109.5
Std. Error	12.3	13.4	5.31	9.57	10.9	13.6	5.45	3.27	6.46	19.1	9.70
Median	89.9	62.9	60.4	99.0	88.2	94.5	96.5	90.4	96.7	95.6	108.5
0.25 Perc.	75.5	55.6	53.5	90.3	80.4	90.5	89.3	83.7	96.7	91.0	95.7
0.75 Perc.	116.2	77.8	67.3	114.8	107.9	117.8	103.5	91.5	110.7	127.6	123.3
Size (N)	6	5	3	3	3	5	3.0	3	7	5	4

Supplementary Figure captions

Fig. E1a: X-ray diffraction pattern of CRM Mess-3 (black trace) showing identified minerals (colored ticks)

Fig. E1b: Normalized X-ray diffraction patterns of CRM Mess-3 before and after NH_4OH extraction (black and red traces, respectively) showing identified minerals (colored ticks)

Fig. E1c: Normalized X-ray diffraction patterns of CRM Mess-3 before and after KOH extraction (black and red traces, respectively) showing identified minerals (colored ticks)

Fig. E1d: Normalized X-ray diffraction patterns of CRM Mess-3 before and after ascorbate extraction (black and red traces, respectively) showing identified minerals (colored ticks)

Fig. E1e: Normalized X-ray diffraction patterns of CRM Mess-3 before and after HCl/HNO_3 extraction (black and red traces, respectively) showing identified minerals (colored ticks)

Fig. E2a: X-ray diffraction pattern of CRM 7002 (black trace) showing identified minerals (colored ticks)

Fig. E2b: Normalized X-ray diffraction patterns of CRM 7002 before and after NH_4OH extraction (black and red traces, respectively) showing identified minerals (colored ticks)

Fig. E2c: Normalized X-ray diffraction patterns of CRM 7002 before and after KOH extraction (black and red traces, respectively) showing identified minerals (colored ticks)

Fig. E2d: Normalized X-ray diffraction patterns of CRM 7002 before and after ascorbate extraction (black and red traces, respectively) showing identified minerals (colored ticks)

Fig. E2e: Normalized X-ray diffraction patterns of CRM 7002 before and after HCl/HNO_3 extraction (black and red traces, respectively) showing identified minerals (colored ticks)

Fig. E3a: X-ray diffraction pattern of sample I-1(0-10m) (black trace) showing identified minerals (colored ticks)

Fig. E3b: Normalized X-ray diffraction patterns of sample I-1(0-10m) before and after NH_4OH extraction (black and red traces, respectively) showing identified minerals (colored ticks)

Fig. E3c: Normalized X-ray diffraction patterns of sample I-1(0-10m) before and after KOH extraction (black and red traces, respectively) showing identified minerals (colored ticks)

Fig. E3d: Normalized X-ray diffraction patterns of sample I-1(0-10m) before and after ascorbate extraction (black and red traces, respectively) showing identified minerals (colored ticks)

Fig. E3e: Normalized X-ray diffraction patterns of sample I-1(0-10m) before and after HCl/HNO_3 extraction (black and red traces, respectively) showing identified minerals (colored ticks)

Fig. E4: X-ray diffraction pattern of nodules from sample I-1(180-200m) (black trace) showing identified minerals (colored ticks)

Fig. E5: Total Hg, $(Hg)_{HCl/HNO3}$, $(Hg)_{residual}$, $(Hg)_{Asco}$, $(Hg)_{NH4OH}$, and $(Hg)_{KOH}$ extractions extraction yield (%) vertical profiles in nodules of pristine soils. Triangles refer to toposequence I, triangles up refers to surface nodules, and

triangle down to deeper horizons III. white and grey filled colours refer to oxisol and ultisol, respectively. Filled triangles refer to sol matrix and hair-crossed symbols refer to nodules.

Fig. E1a. X-ray diffraction pattern of CRM Mess-3 (black trace) showing identified minerals (colored ticks)

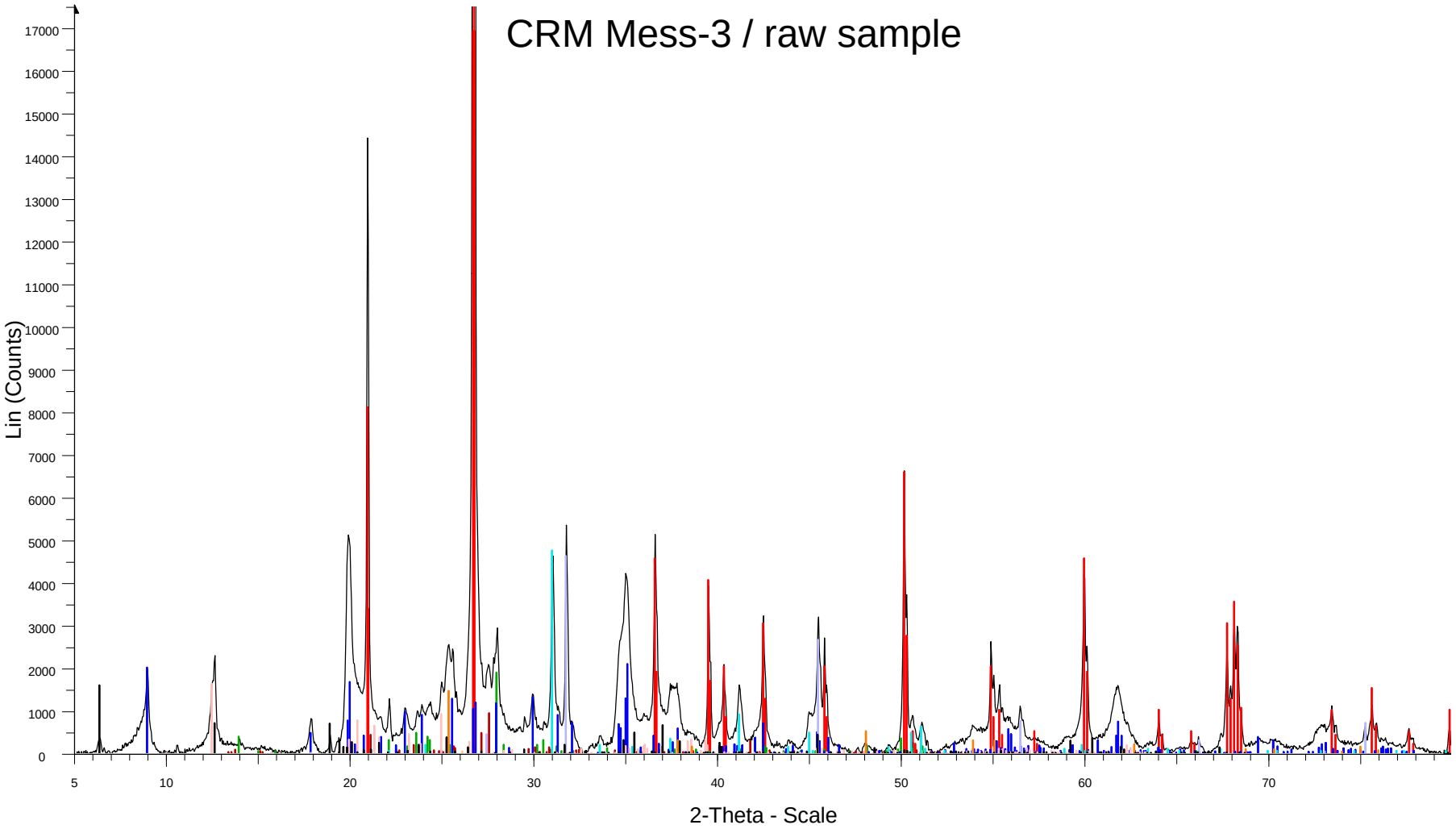

Fig. E1b. Normalized X-ray diffraction patterns of CRM Mess-3 before and after NH_4OH extraction (black and red traces, respectively) showing identified minerals (colored ticks)

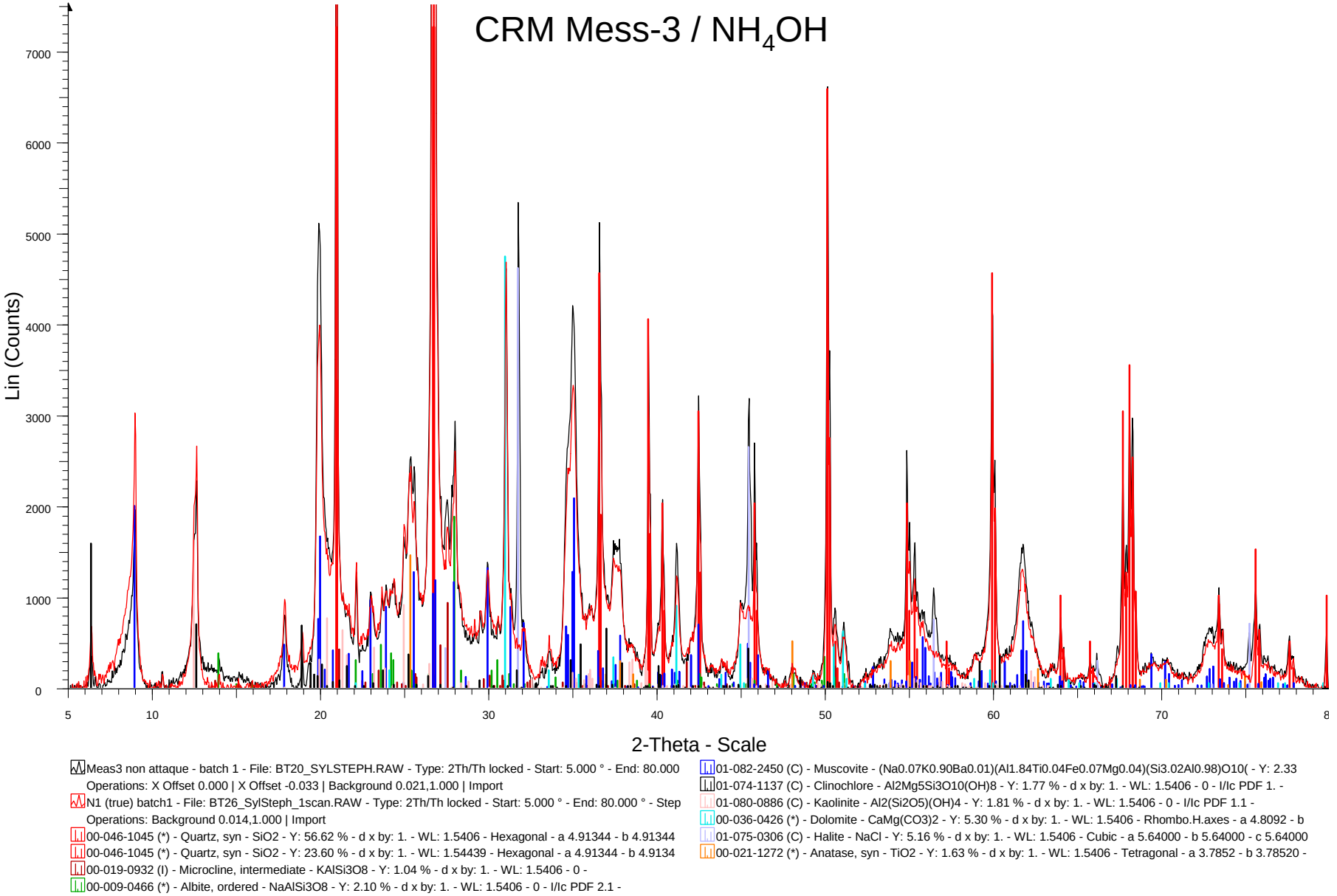

Fig. E1c. Normalized X-ray diffraction patterns of CRM Mess-3 before and after KOH extraction (black and red traces, respectively) showing identified minerals (colored ticks)

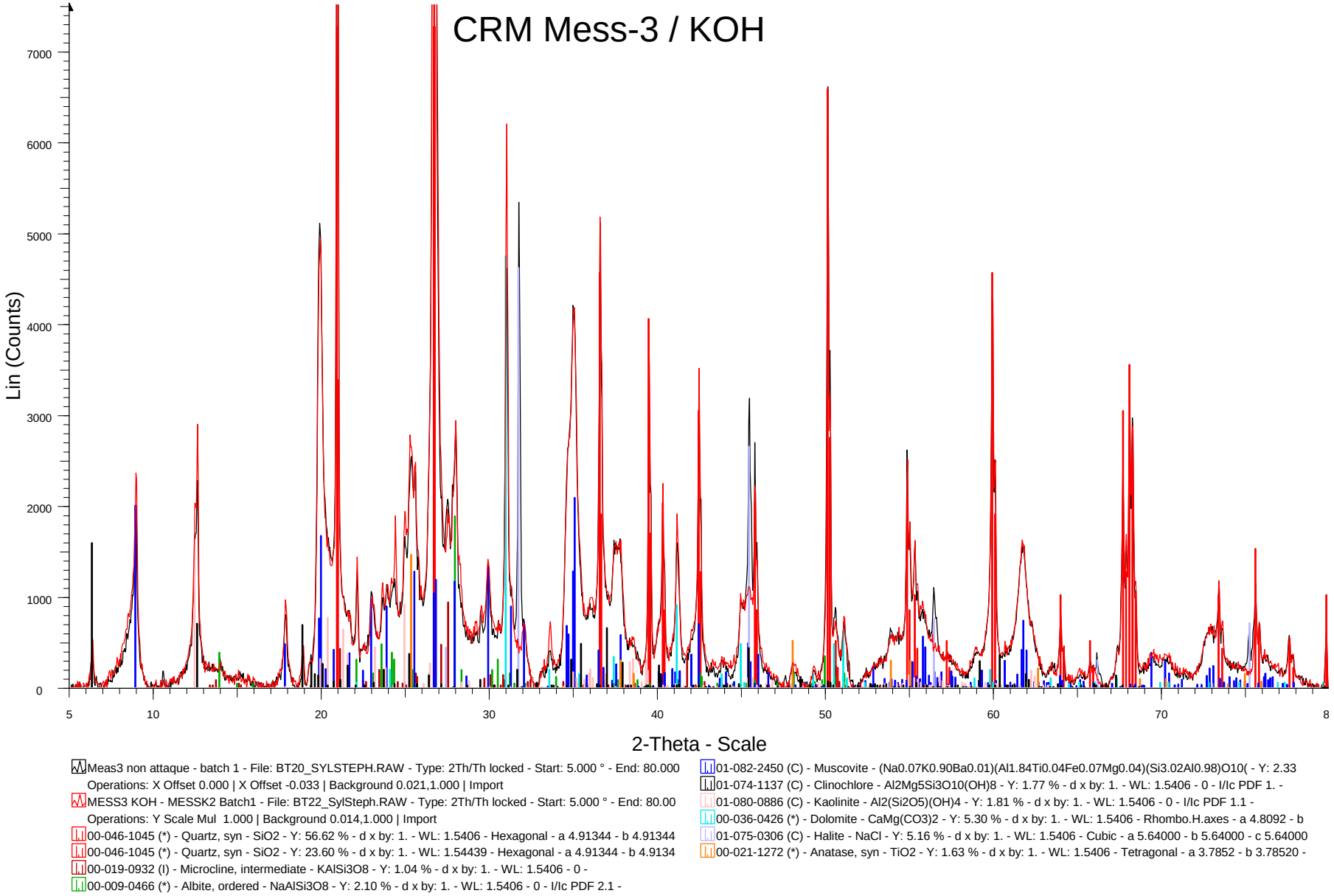

Fig. E1d. Normalized X-ray diffraction patterns of CRM Mess-3 before and after ascorbate extraction (black and red traces, respectively) showing identified minerals (colored ticks)

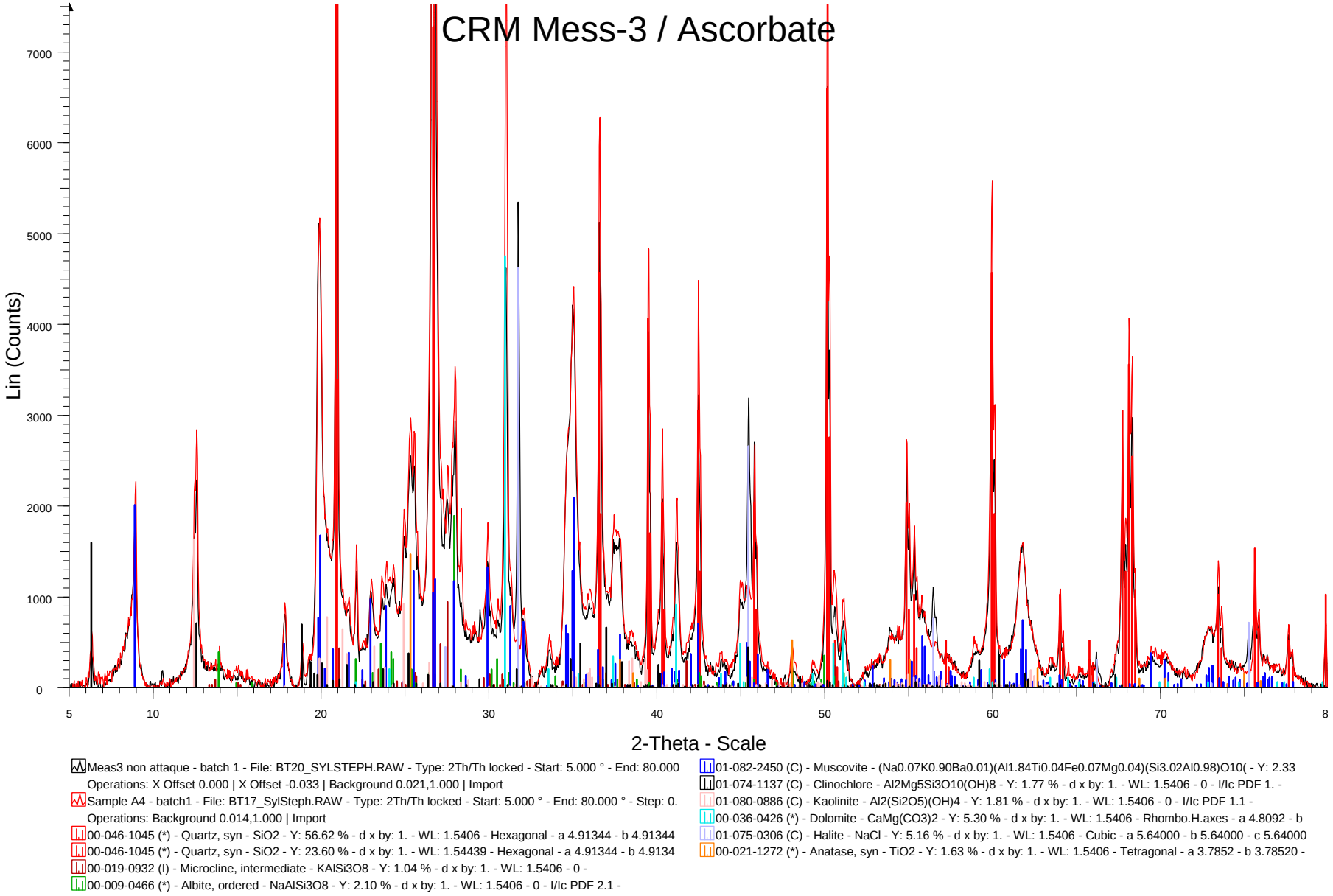

Fig. E1e. Normalized X-ray diffraction patterns of CRM Mess-3 before and after HCl extraction (black and red traces, respectively) showing identified minerals (colored ticks)

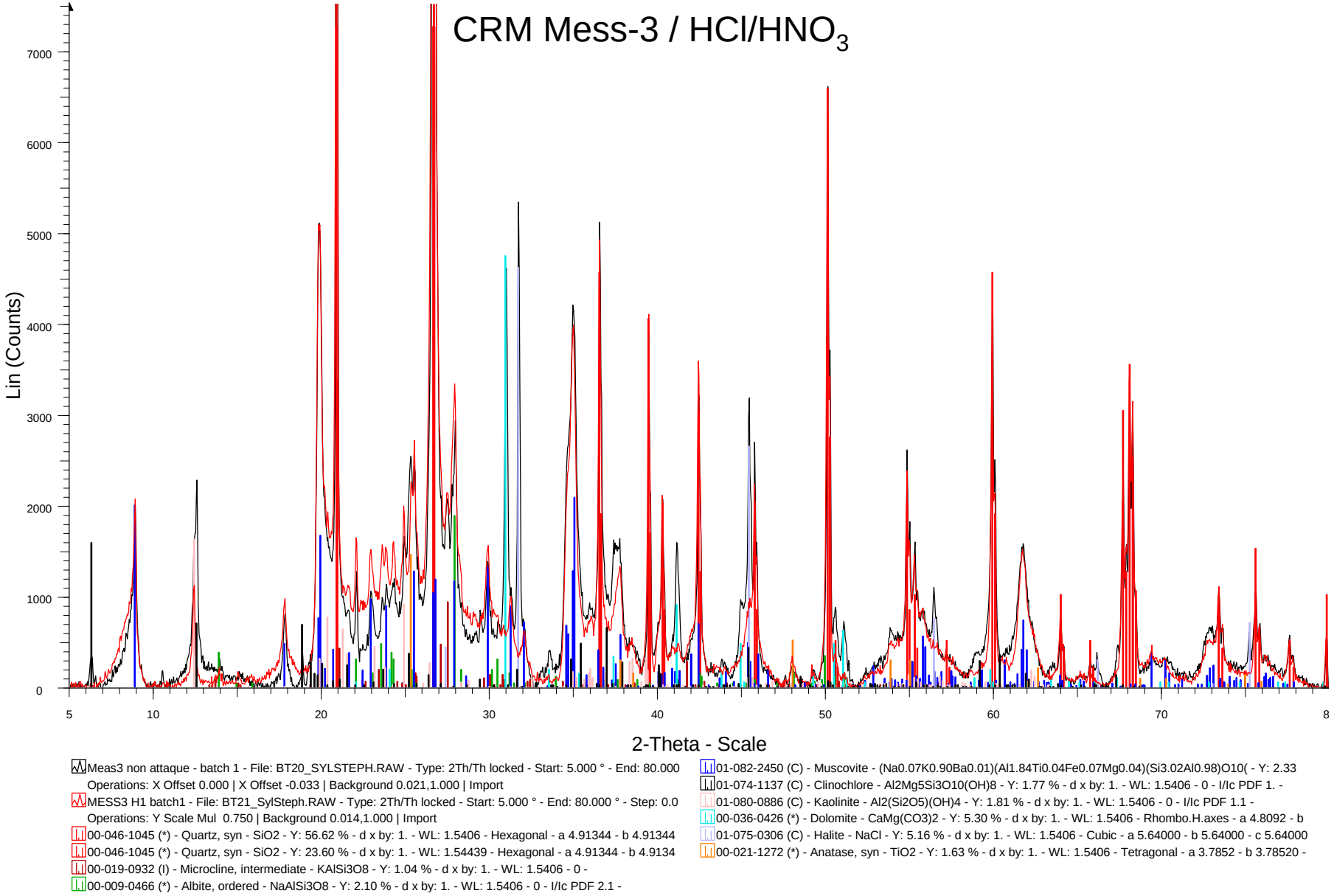

Fig. E2a. X-ray diffraction pattern of CRM 7002 (black trace) showing identified minerals (colored ticks)

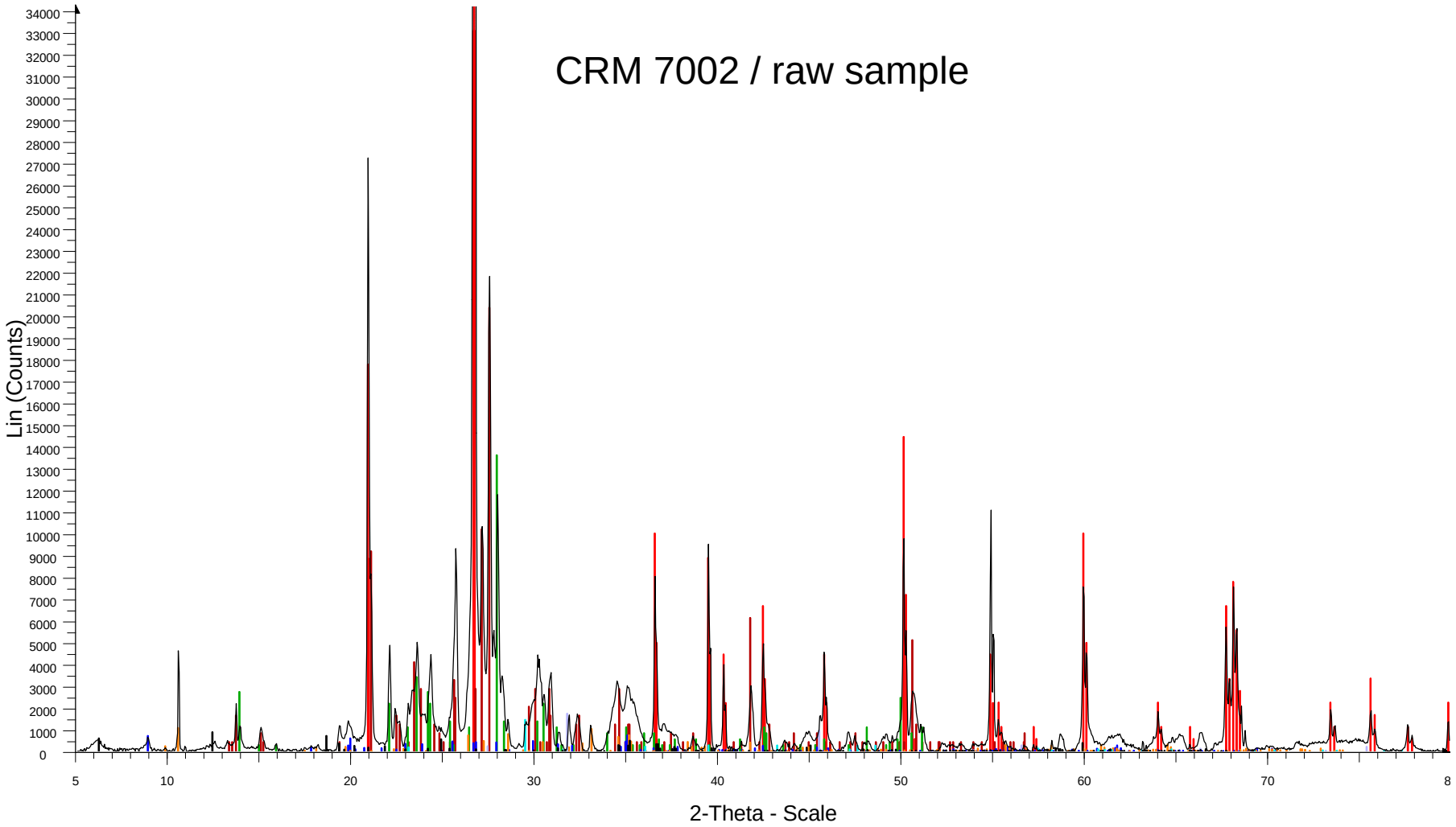

Fig. E2b. Normalized X-ray diffraction patterns of CRM 7002 before and after NH_4OH extraction (black and red traces, respectively) showing identified minerals (colored ticks)

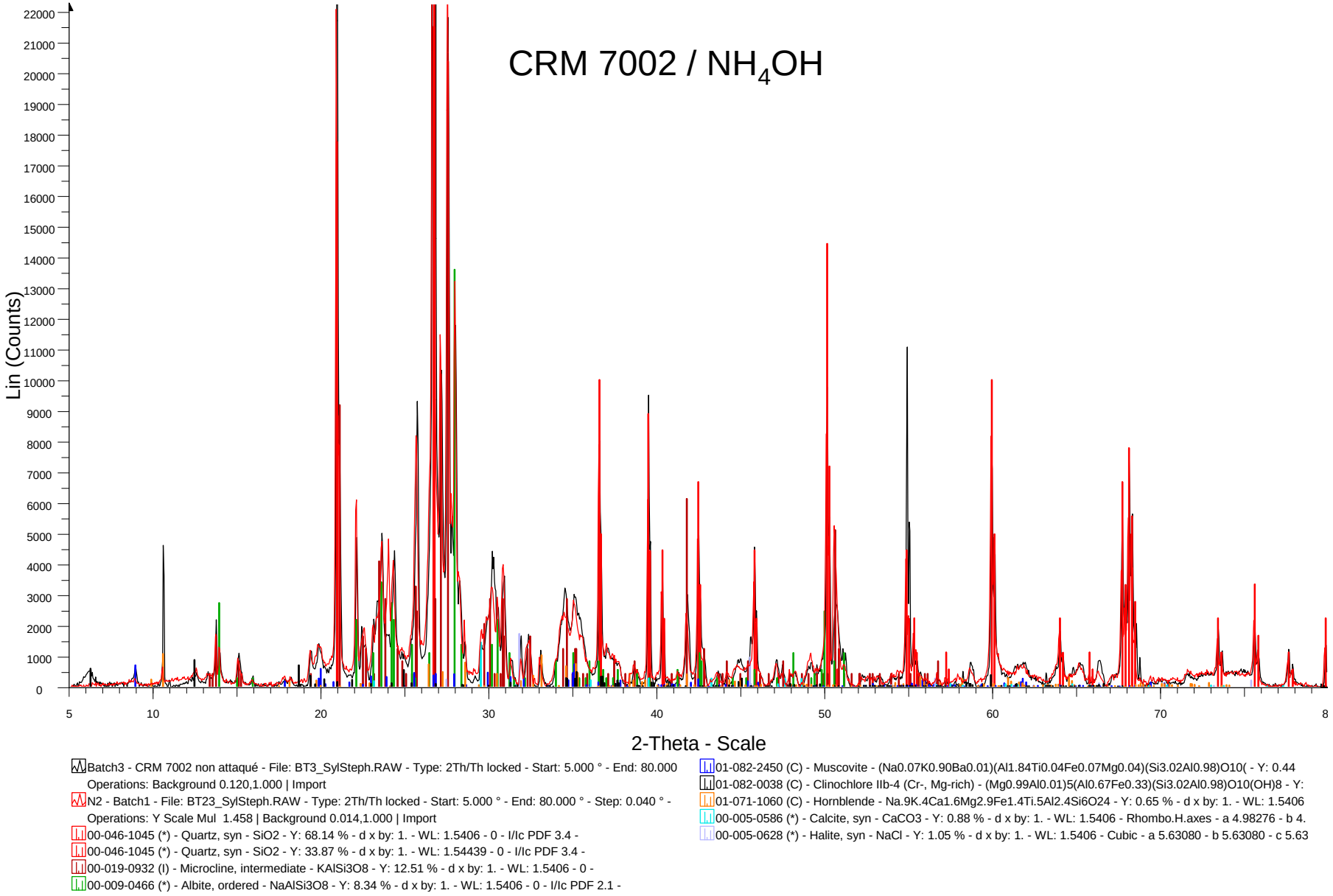

Fig. E2c. Normalized X-ray diffraction patterns of CRM 7002 before and after KOH extraction (black and red traces, respectively) showing identified minerals (colored ticks)

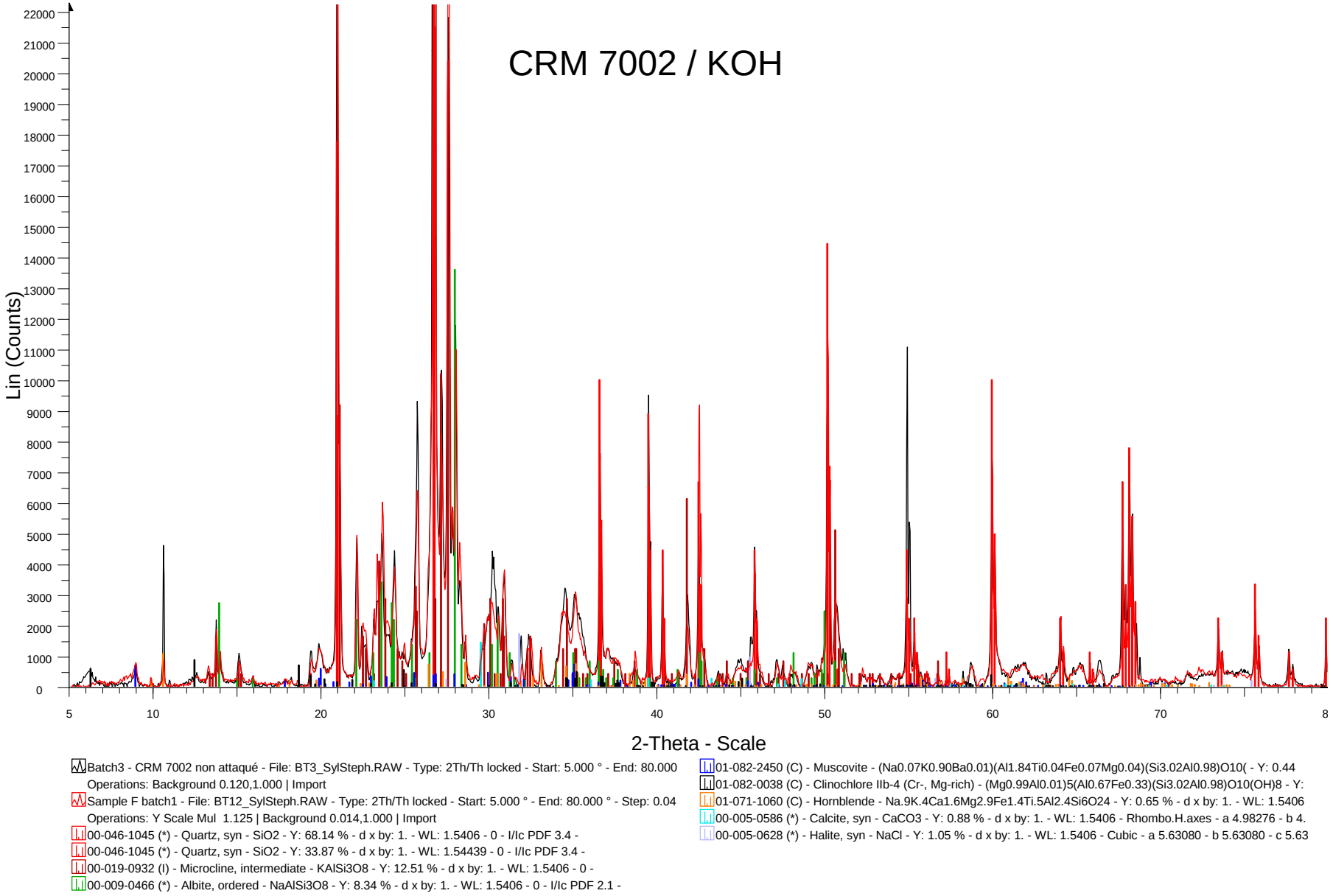

Fig. E2d. Normalized X-ray diffraction patterns of CRM 7002 before and after ascorbate extraction (black and red traces, respectively) showing identified minerals (colored ticks)

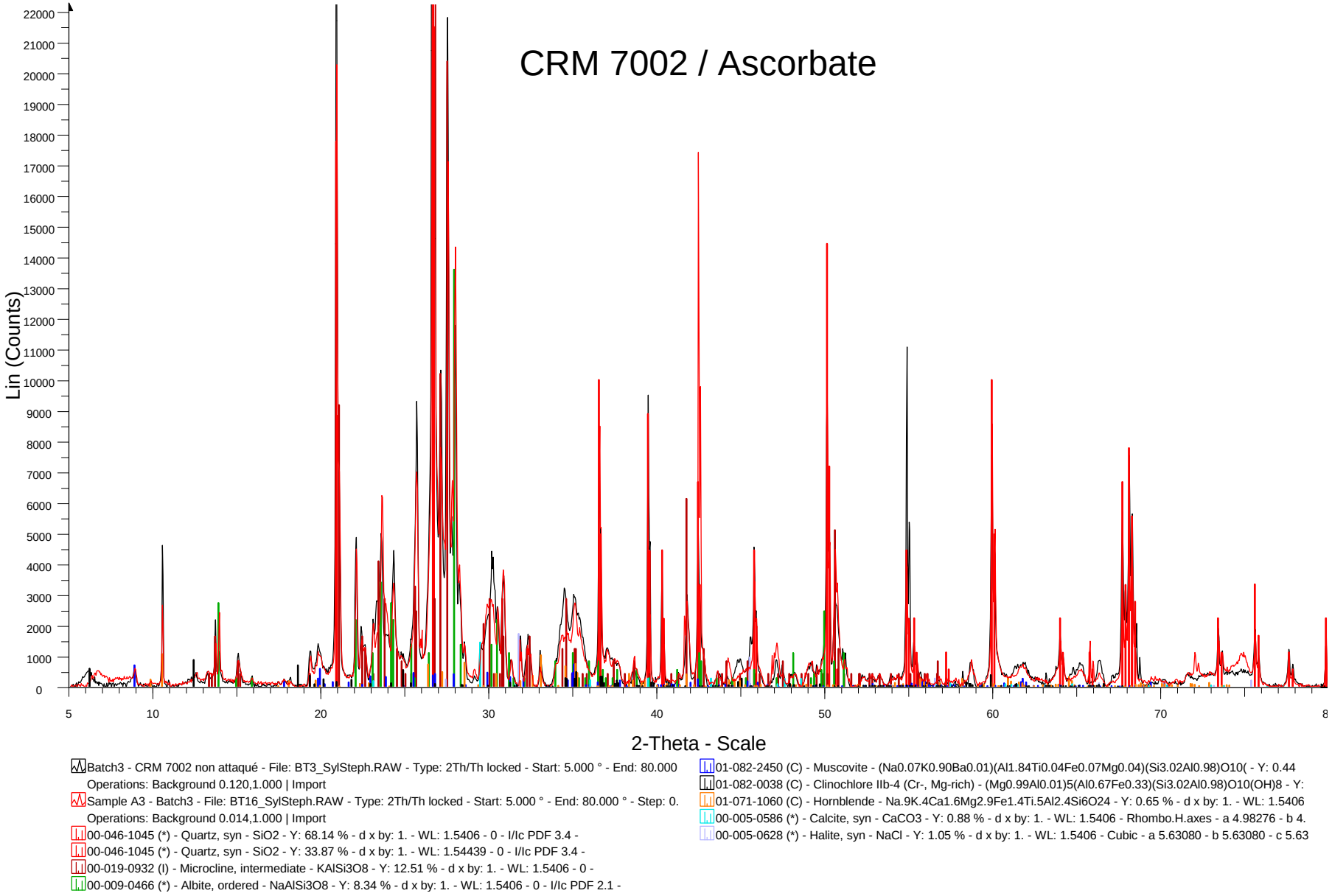

Fig. E2e. Normalized X-ray diffraction patterns of CRM 7002 before and after HCl extraction (black and red traces, respectively) showing identified minerals (colored ticks)

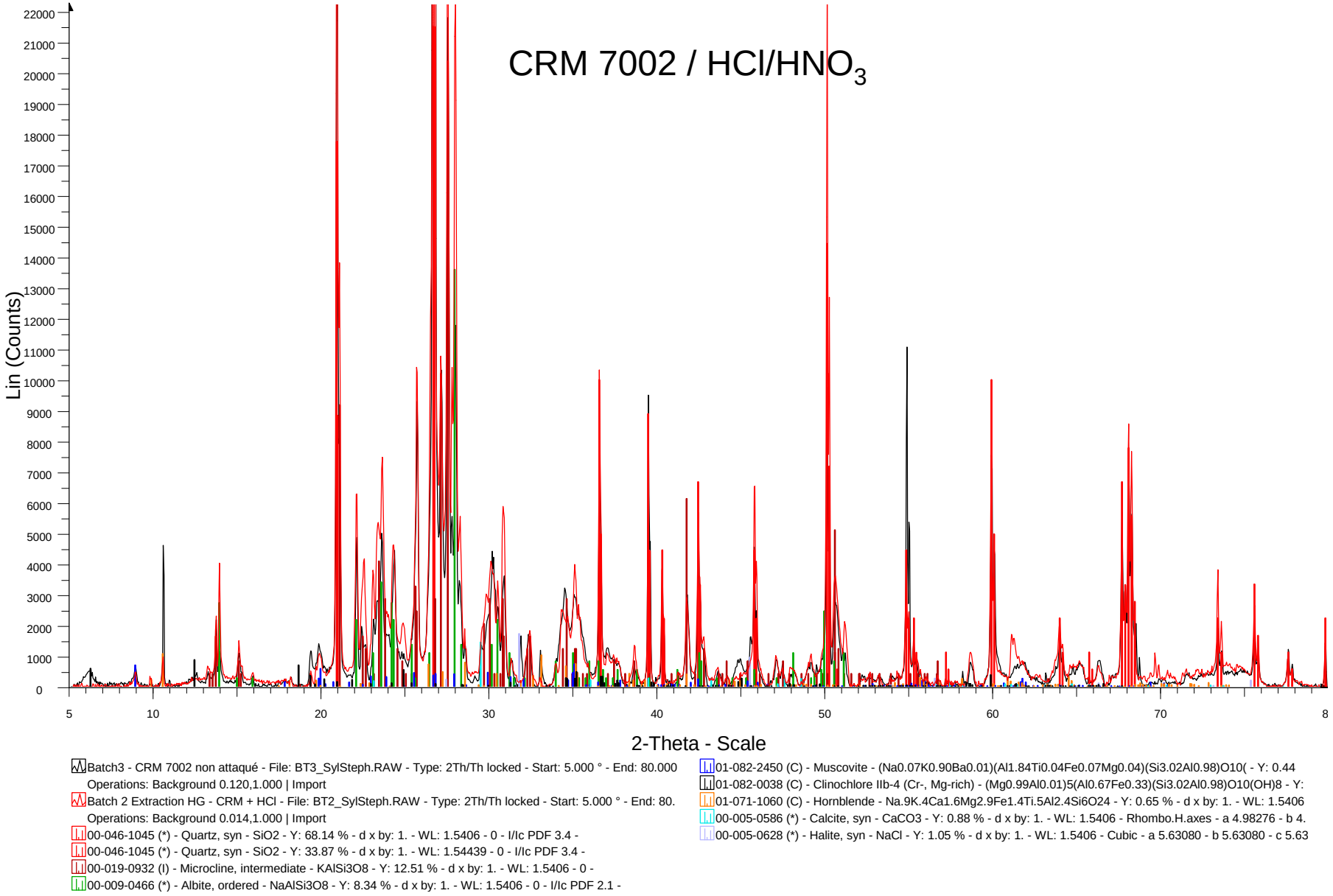

Fig. E3a. X-ray diffraction pattern of sample I-1(0-10m) (black trace) showing identified minerals (colored ticks)

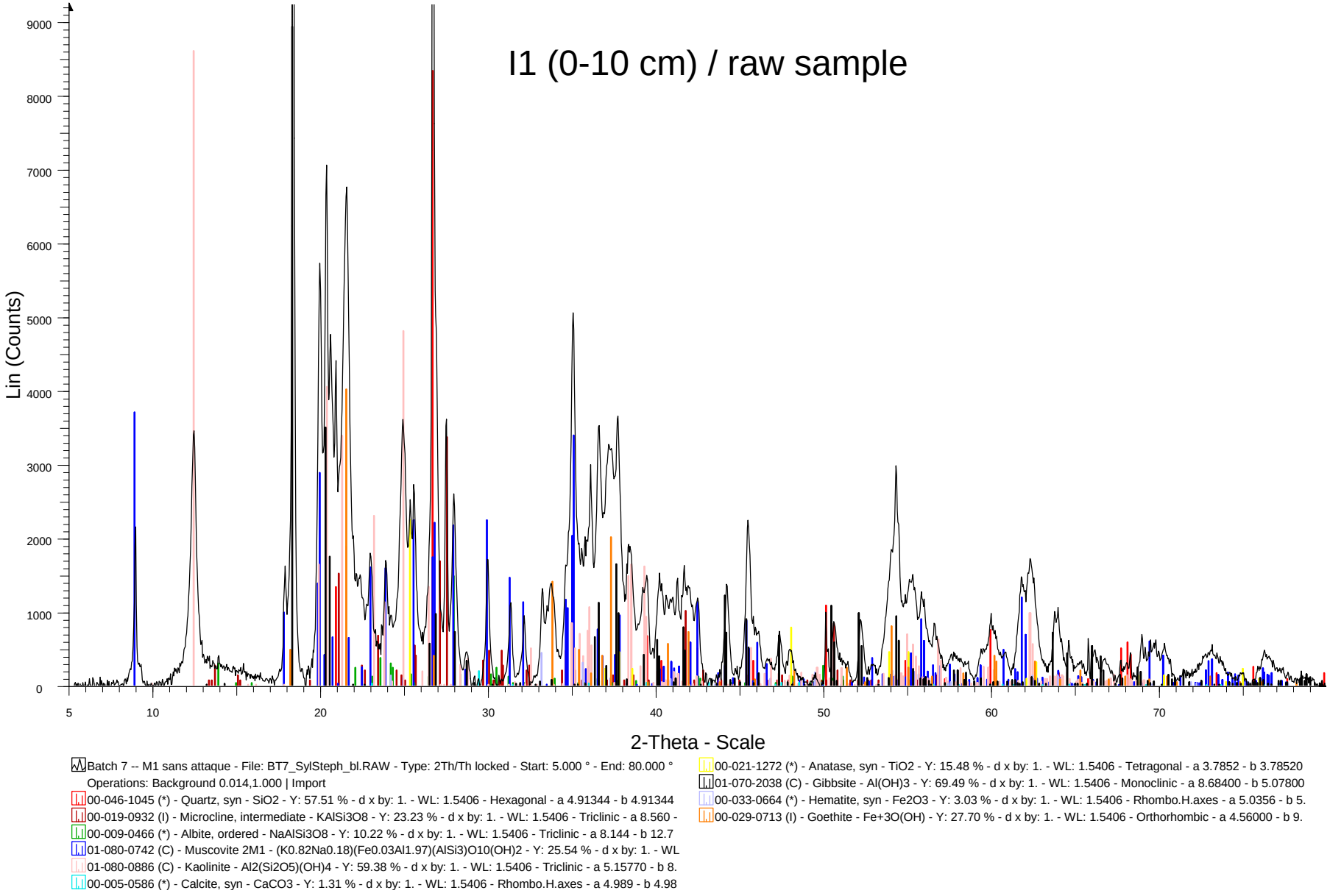

Fig. E3b. Normalized X-ray diffraction patterns of sample I-1(0-10m) before and after NH_4OH extraction (black and red traces, respectively) showing identified minerals (colored ticks)

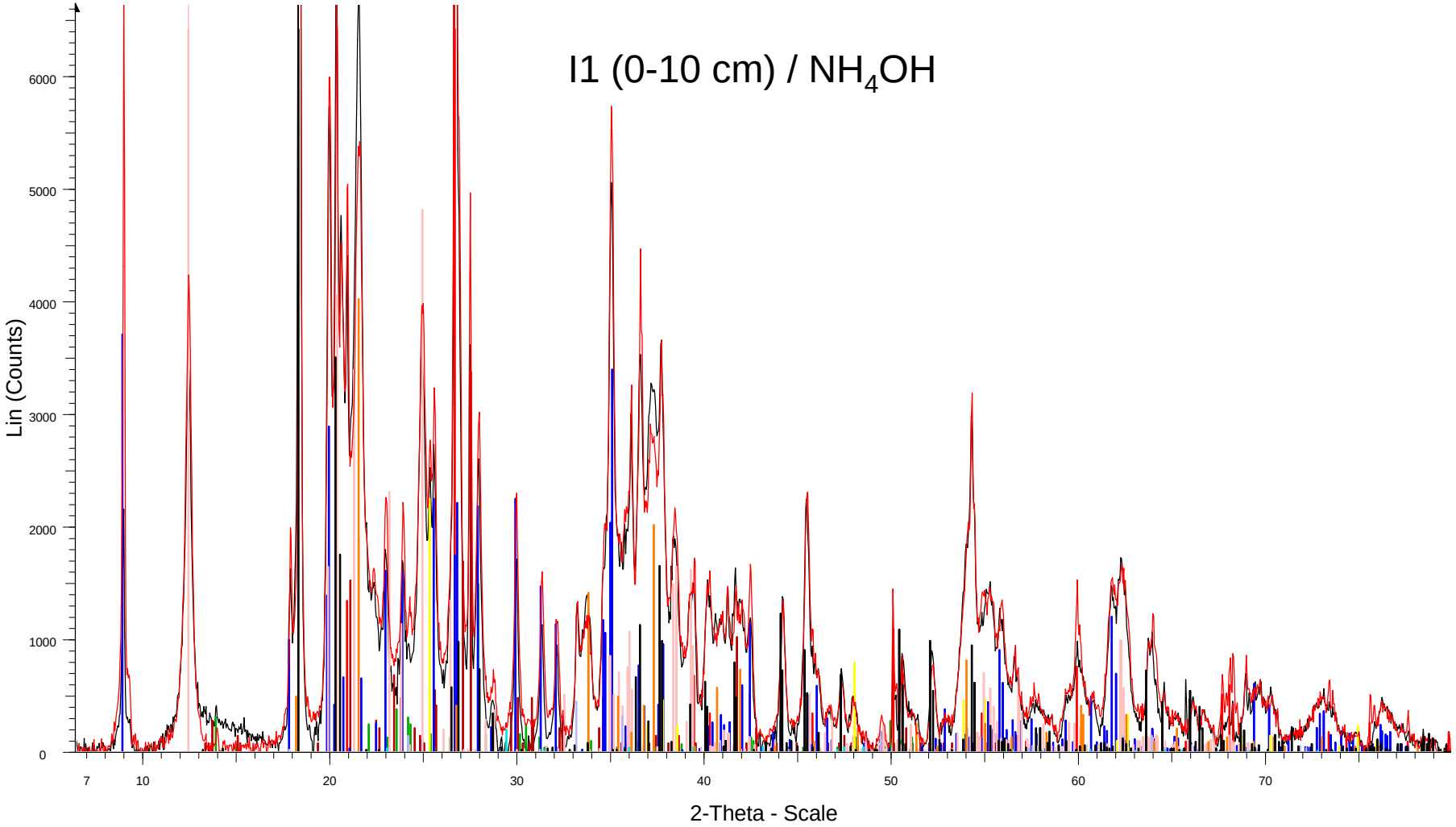

Fig. E3c. Normalized X-ray diffraction patterns of sample I-1(0-10m) before and after KOH extraction (black and red traces, respectively) showing identified minerals (colored ticks)

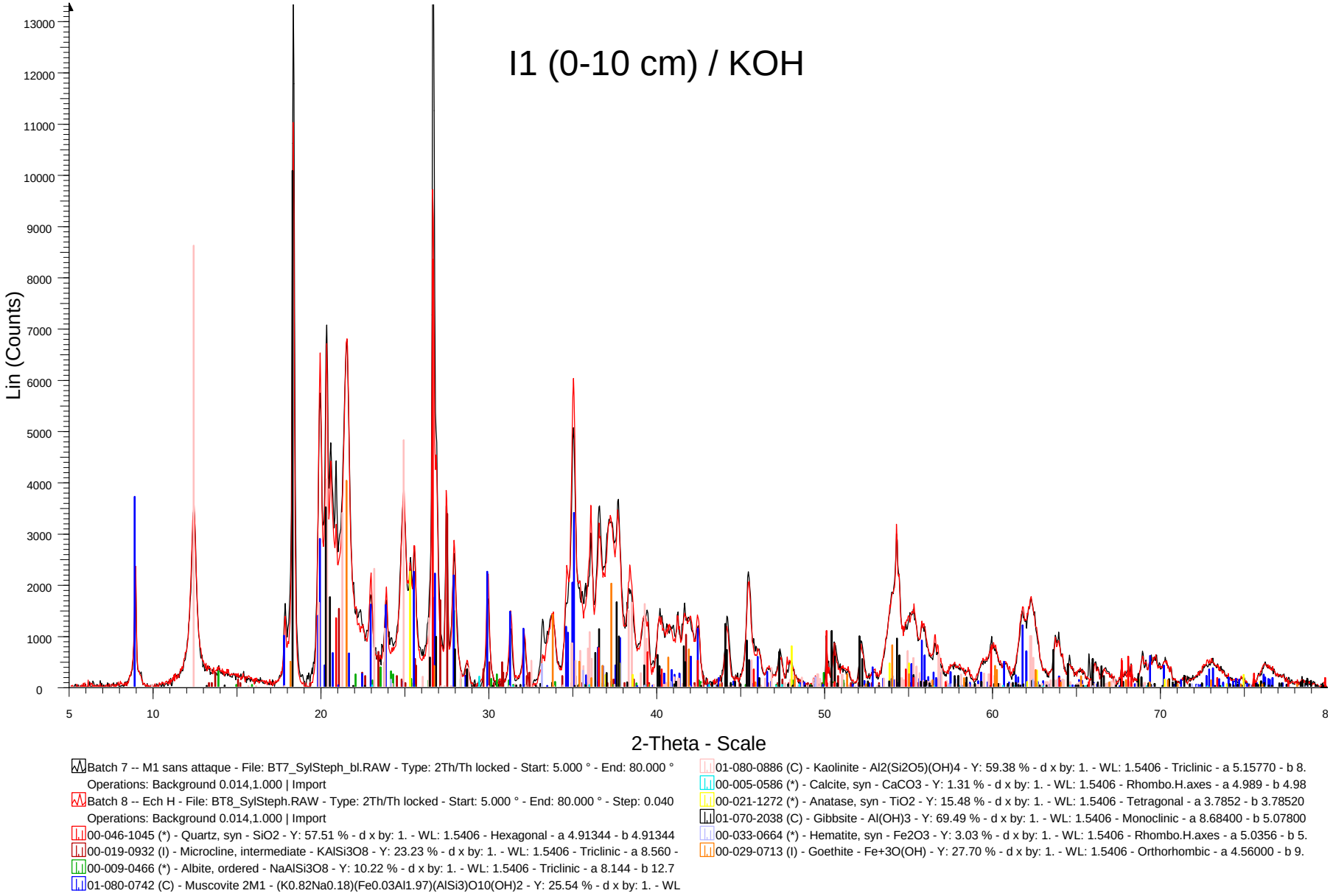

Fig. E3d. Normalized X-ray diffraction patterns of sample I-1(0-10m) before and after ascorbate extraction (black and red traces, respectively) showing identified minerals (colored ticks)

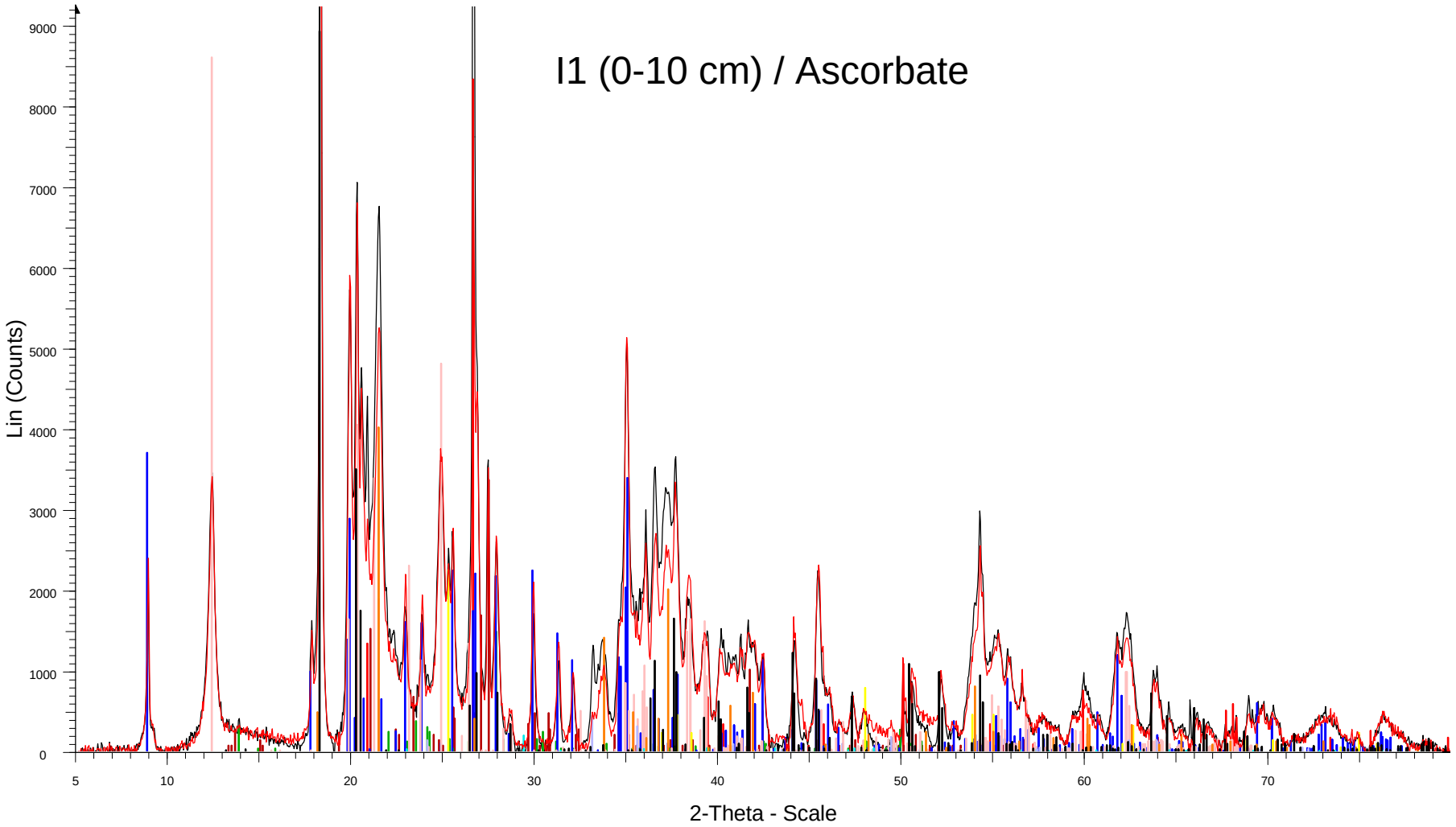

Fig. E3e. Normalized X-ray diffraction patterns of sample I-1(0-10m) before and after HCl extraction (black and red traces, respectively) showing identified minerals (colored ticks)

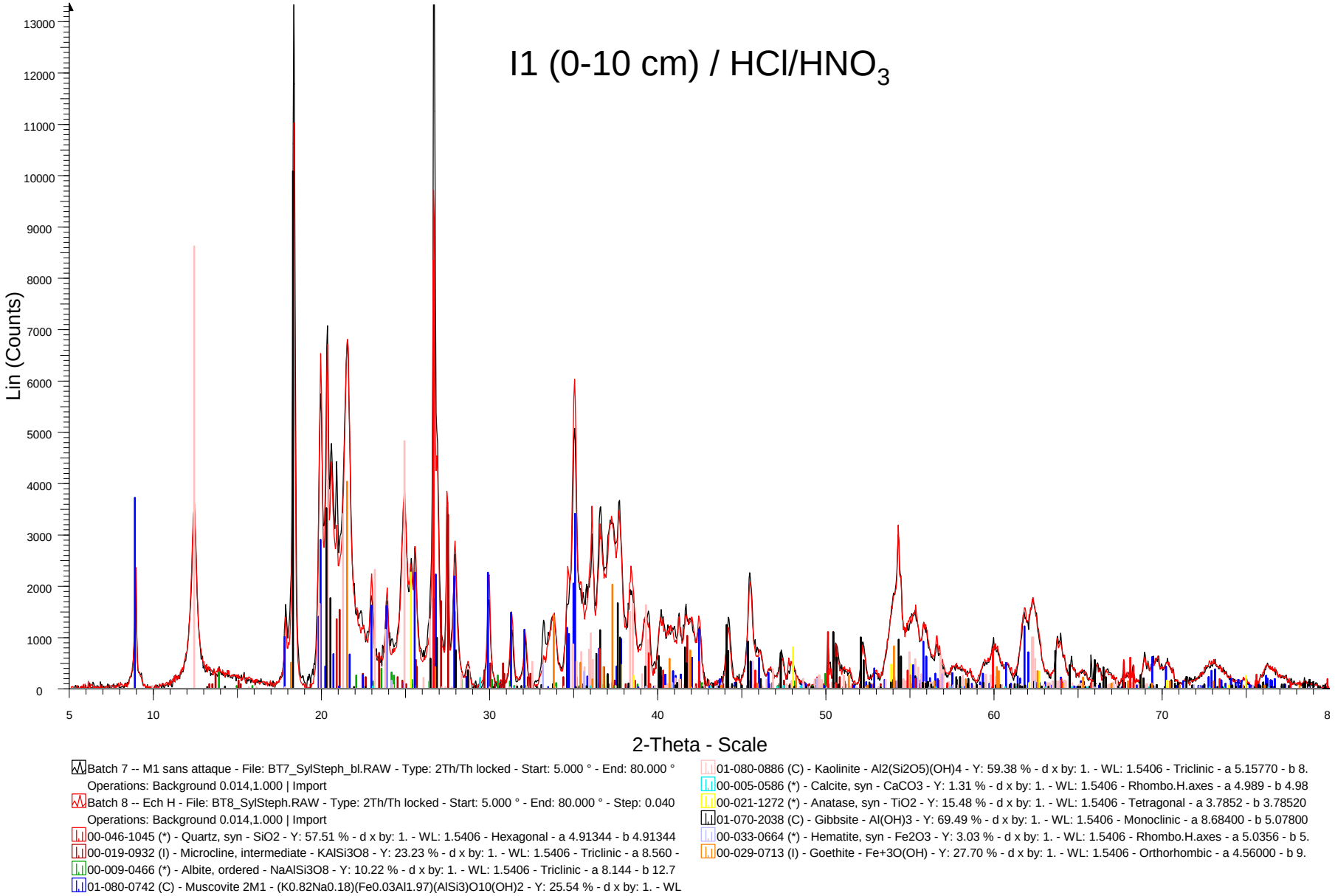

Fig. E4. X-ray diffraction pattern of nodules from sample I-1(180-200m) (black trace) showing identified minerals (colored ticks)

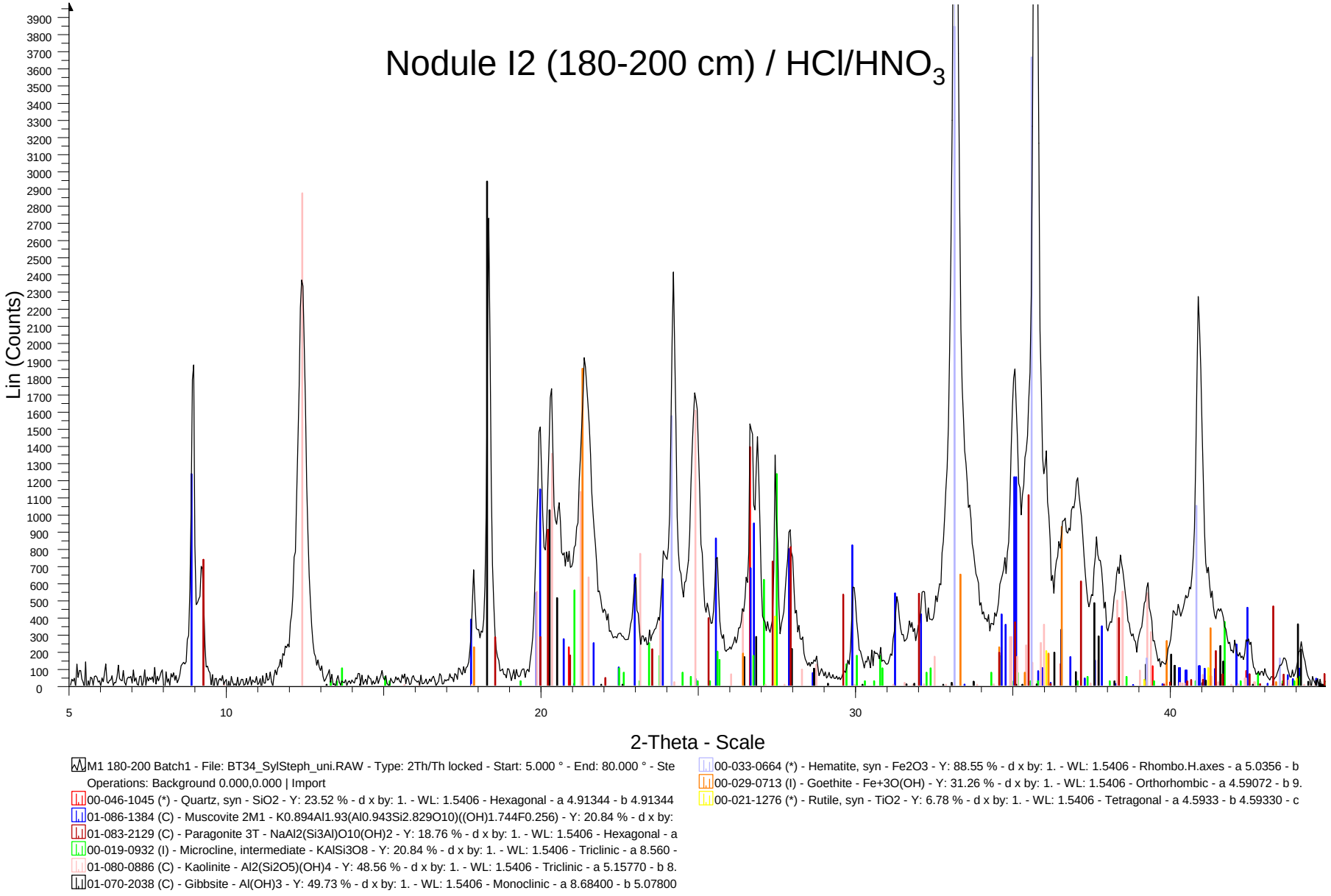

Fig. E5.

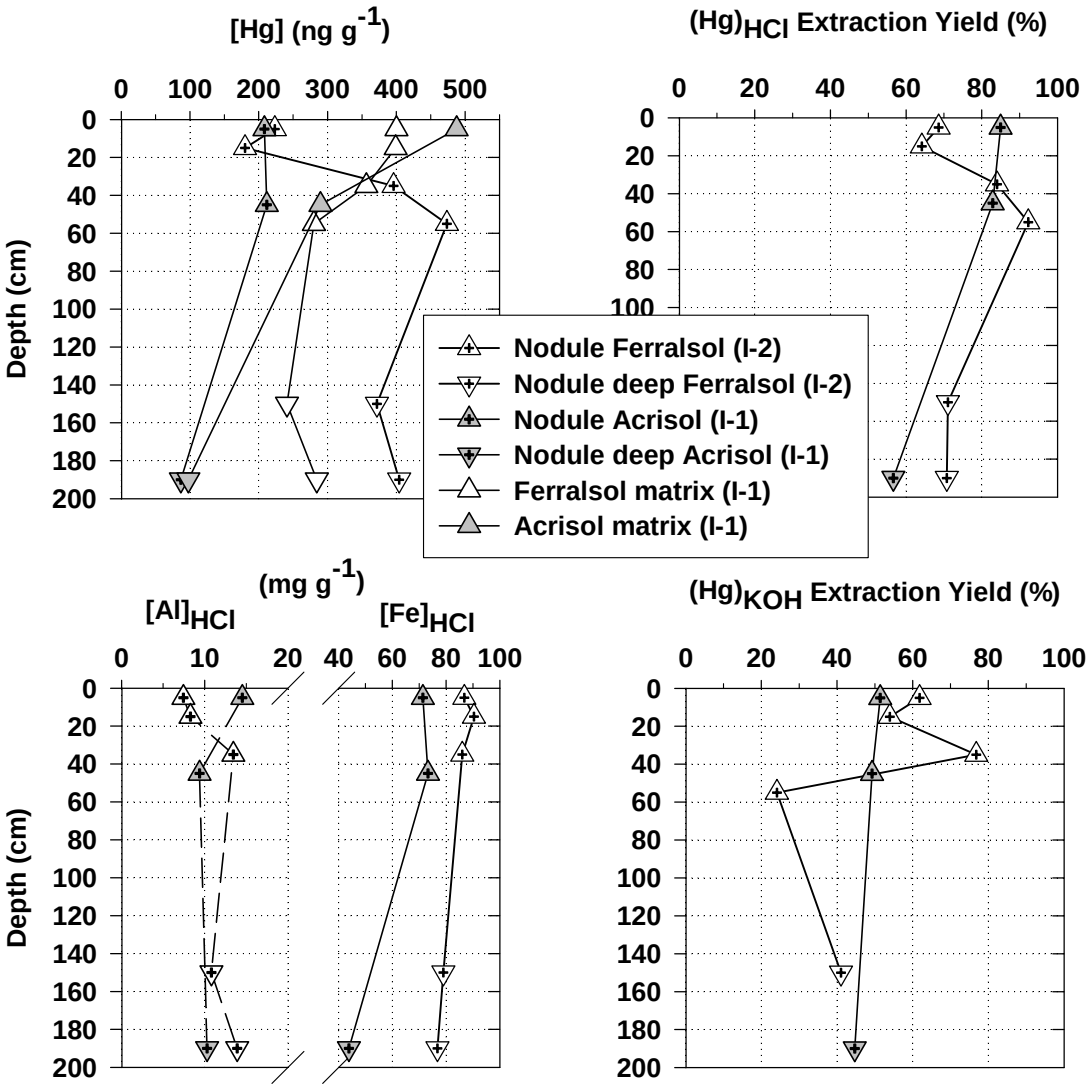
[Hg] (ng g-1)
(Hg)HCl Extraction Yield (%)
Depth (cm)
Nodule Ferralsol (I-2)
Nodule deep Ferralsol (I-2)
Nodule Acrisol (I-1)
Nodule deep Acrisol (I-1)
Ferralsol matrix (I-1)
Acrisol matrix (I-1)
(mg g-1)
[Al]HCl
[Fe]HCl
(Hg)KOH Extraction Yield (%)